

AdaGC: Enhancing LLM Pretraining Stability via Adaptive Gradient Clipping

Guoxia Wang^{1*} Shuai Li^{1*} Congliang Chen² Jinle Zeng¹ Jiabin Yang¹ Dianhai Yu¹ Yanjun Ma¹ Li Shen³

Abstract

Loss spikes remain a persistent obstacle in large-scale language model pretraining. While previous research has attempted to identify the root cause of loss spikes by investigating individual factors, we observe that, in practice, such spikes are typically triggered by the confluence of heterogeneous factors. Empirically, loss spikes may arise from a combination of data outliers, hardware or transient computational faults, numerical precision issues, and hyperparameter settings. Regardless of the underlying cause, these spikes manifest as unstable optimizer updates, as abnormal gradients contaminate both first- and second-moment states. In this paper, we propose a principled gradient-centric remedy: AdaGC, an adaptive tensor gradient clipping scheme that mitigates such contamination by bounding gradient norms relative to a tensor-wise exponential moving average of their historical clipped values. AdaGC is optimizer-agnostic, introduces negligible memory overhead, and reduces communication costs compared to GlobalGC, particularly in hybrid-parallel distributed training environments. Experiments on Llama-2 7B, Mixtral 8×1B, and ERNIE 10B-A1.4B demonstrate that AdaGC robustly eliminates training instabilities, consistently reducing spike scores to zero for all models and improving downstream accuracy over GlobalGC by 1.32%, 1.27%, and 2.48%, respectively. Furthermore, AdaGC seamlessly integrates with optimizers such as Muon and Lion, consistently yielding higher average accuracy and zero spike scores.

1. Introduction

The rapid scaling of large language models (LLM) has introduced new challenges in pretraining stability, often mani-

*Equal contribution ¹Baidu Inc., China ²The Chinese University of Hong Kong (Shenzhen), China ³Shenzhen Campus of Sun Yat-sen University, China. Correspondence to: Dianhai Yu <yudi-anhai@baidu.com>, Li Shen <mathshenli@gmail.com>.

Preprint.

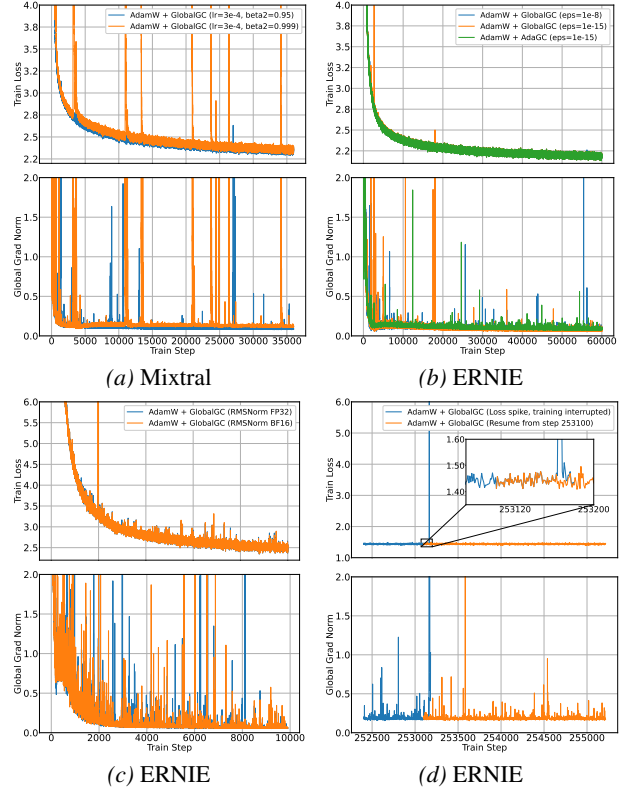


Figure 1. Reproduced cases of loss spikes and mitigation via resuming. Loss spikes are triggered by (a) increasing β_2 or (b) reducing ϵ in AdamW, (c) using lower-precision RMSNorm, even under global gradient clipping, and (d) are resolved by resuming due to stochasticity in FlashAttention backward passes.

festing as abrupt loss spikes or transient divergences across a wide range of model architectures and data scales (Chowdhery et al., 2023; Touvron et al., 2023; Liu et al., 2024; Team et al., 2025; Baidu-ERNIE-Team, 2025). Despite extensive empirical studies, the fundamental causes of these instabilities remain elusive. Recent research, alongside our own analyses, indicates that loss spikes can arise from a variety of sources, including: (i) data quality issues (Chowdhery et al., 2023); (ii) hardware or transient computational faults (Su, 2025); (iii) variations in numerical precision (for example, FP32 typically offers greater robustness than BF16, whereas FP8 can sometimes enhance stability by suppressing outlier values via implicit quantization (Han, 2024; Liu et al., 2024)); and (iv) the selection of optimizer and layer normalization hyperparameters, such as the ϵ pa-

Table 1. Common sources of loss spikes in LLM pretraining, with typical triggers and practical mitigations.

Source	Typical trigger	Common mitigation
Data quality	Noisy/ill-formed samples	Resume and skip data batches
Hardware / transient faults	GPU silent errors	Fault tolerance and machine replacement
Numerical precision	Activation outlier	BF16 to FP32 or blockwise quantization
Optimizer / LN hyperparams	AdamW/RMSNorm ϵ ; AdamW β_2	Careful hyperparameter selection

parameter in RMSNorm or AdamW, and β_2 in AdamW (Ma et al., 2021; Cattaneo & Shigida, 2025; Bai et al., 2025). For instance, we observe that increasing β_2 or decreasing ϵ in AdamW can trigger loss spikes, whereas increasing the precision of RMSNorm from BF16 to FP32 significantly improves stability. In summary, Table 1 presents the common sources, typical triggers, and practical mitigations for loss spikes identified from both previous studies and our experimental findings, while Figure 1 demonstrates several representative cases we have reproduced.

Although the upstream causes of instability are diverse and often subtle, these events consistently converge at the optimizer level, manifesting as abnormal gradients. Such outlier gradients are incorporated into the optimizer’s first- and second-moment estimates, thereby corrupting parameter updates and propagating instability through subsequent training. Notably, we find that even resuming interrupted training (while keeping the random seed and data unchanged) can mitigate a loss spike, merely due to the stochastic nature of dQ , dK , and dV in FlashAttention (Dao, 2023) (see Figure 1d). This observation further suggests that, in certain model states, even minute numerical differences can trigger a loss spike, with gradient outliers playing a critical role in both the initiation and propagation of instabilities during optimizer state updates.

While the slight stochasticity introduced by FlashAttention can sometimes circumvent a loss spike, repeatedly interrupting and resuming training imposes substantial computational overhead. Given that these instabilities stem from diverse upstream causes but ultimately converge at the optimizer level, our work *does not attempt to identify the precise root causes*. Instead, we adopt a **gradient-centric** perspective: irrespective of the initial trigger, loss spikes consistently arise when outlier gradients contaminate the optimizer states. Therefore, by preventing such gradients from entering the first- and second-moment accumulators, we provide a unified and effective strategy to mitigate training instability.

A standard mitigation strategy is global gradient clipping (GlobalGC), which bounds the global ℓ_2 norm of the aggregated gradient. However, this approach is fundamentally mismatched to modern large-scale pretraining in two key respects: (1) *Temporal mismatch*: The optimal global clipping threshold typically decreases over the course of training; a fixed threshold risks under-clipping in later phases. (2)

Spatial mismatch: Gradient statistics and rare spikes vary asynchronously across different parameter tensors, making a single global threshold insufficient—protecting one tensor may under-serve or over-constrain others.

To address these challenges, we introduce *Adaptive Gradient Clipping based on Local Gradient Norm* (AdaGC): a simple, per-tensor clipping rule that leverages an EMA of each tensor’s historical gradient norm as a reference. Each tensor’s gradient is clipped relative to its own EMA, preventing transient outliers from contaminating the first- and second-moment accumulators and, ultimately, the parameter updates. A brief warm-up period applies global clipping and initializes the EMA to avoid early overestimation. AdaGC is optimizer-agnostic and can be seamlessly integrated with AdamW, Lion, and Muon. Our main contributions are as follows:

- **A unified, gradient-centric perspective**: We clarify how loss spikes universally propagate via abnormal gradients polluting optimizer states, irrespective of their origin, motivating intervention at the gradient level prior to moving-average accumulation.
- **An adaptive, per-tensor clipping rule**: By tracking each tensor’s gradient norm statistics with an EMA, AdaGC provides both temporal adaptivity and spatial specificity, suppressing outliers while minimally disturbing typical learning dynamics.
- **System efficiency**: We analyze computational and communication overhead, showing that AdaGC reduces communication relative to GlobalGC under hybrid parallel distributed training.
- **Empirical validation at scale**: On Llama-2 7B, Mixtral $8\times 1B$, and ERNIE 10B-A1.4B models, AdaGC robustly eliminates training instabilities and improves accuracy compared to GlobalGC by +1.32%, +1.27%, and +2.48%, respectively. The method is similarly effective with AdamW, Lion, and Muon optimizers.

2. Related Work

Stability in large-scale pretraining: Dozens of approaches address instability during large-model pretraining, including: architectural advances (Pre-LN (Xiong et al., 2020),

Table 2. Comparison of major gradient/update clipping methods for stability. Here, θ_t denotes the model parameters, g_t the gradients, Δ_t the optimizer update, η_t the learning rate, λ_{abs} the absolute threshold, and λ_{rel} the relative threshold.

Method	Algorithm	Gradient	Update	Granularity	Threshold Type
GlobalGC (Pascanu et al., 2013)	$\min\{1.0, \lambda_{abs} \frac{1}{\ g_t\ }\}$	✓	✗	Global	Fixed constant
ClipByValue	$clamp(-\lambda_{abs}, \lambda_{abs})$	✓	✗	Element	Fixed constant
AGC (Brock et al., 2021)	$\min\{1.0, \lambda_{rel} \frac{\ \theta_t\ }{\ \Delta_t\ }\}$	✗	✓	Unit	Weight ℓ_2 norm
Clippy (Tang et al., 2023)	$\min\{1.0, \min(\frac{\lambda_{rel}\ \theta_t\ _{\infty} + \lambda_{abs}}{\eta_t * \ \Delta_t\ _{\infty}})\}$	✗	✓	Tensor	Weight ℓ_{∞} norm
AdaGC (ours)	$\min\{1.0, \lambda_{rel} \frac{\gamma_{t-1,i}}{\ g_{t,i}\ }\}$ $\gamma_{t,i} = \beta\gamma_{t-1,i} + (1 - \beta)\ g_{t,i}\ $	✓	✗	Tensor	EMA of gradient norm

RMSNorm (Zhang & Sennrich, 2019)), careful initialization (Nguyen & Salazar, 2019; Takase et al., 2023; Nishida et al., 2024), auxiliary loss terms (Max-z loss (Yang et al., 2023)). Recent work (OLMo et al., 2024) also explores combining multiple stabilization strategies. These measures improve average stability but do not directly prevent abnormal gradients from corrupting optimizer states.

Gradient/Update Clipping: Gradient and update clipping achieve stability by limiting the magnitude of gradients and parameter updates, preventing excessively large weight updates. Global gradient clipping (Pascanu et al., 2013) is prevalent, with innovative approaches like AGC (Brock et al., 2021) and Clippy (Tang et al., 2023), which use model weights to adjust the clipping threshold. The SPAM (Huang et al., 2025) method stabilizes the model training process by introducing a momentum reset mechanism and an element-wise gradient clipping strategy based on second-moment estimation. Alternatives like Adafactor (Shazeer & Stern, 2018), StableAdamW (Wortsman et al., 2023), and LAMB (You et al., 2019) offer update clipping techniques better suited for stability training of large-scale models. Nonetheless, a significant number of loss spikes still occur during the training of large language models, even with the application of these methodologies. Due to our gradient-centric perspective, we focus our discussion on *clipping-based* methods. These methods fall into two categories: *value-based* approaches, which truncate individual gradient components exceeding a predefined limit, and *norm-based* approaches, which rescale the entire gradient vector only when its overall magnitude exceeds a threshold. AdaGC belongs to the *norm-based* category, leveraging adaptive per-tensor norm thresholds to stabilize training. For a comparative summary, see Table 2.

3. Motivation: From Root-Cause Diversity to a Unified Gradient-Centric Remedy

Through a series of experiments (see Figure 1 and Figure 2), we observe that loss spikes encountered under diverse settings consistently coincide with abrupt fluctuations in the gradient norm. Comparative analyses further reveal limi-

tations of existing methods such as GlobalGC, AGC, and Clippy: GlobalGC’s static global threshold cannot detect or suppress localized abnormal gradients, allowing outliers to contaminate optimizer states and trigger instability. AGC and Clippy focus on controlling parameter updates, leaving internal moments vulnerable to large gradient outliers.

As discussed in the Introduction (Section 1), loss spikes typically result from a combination of multiple factors. While the specific triggers may vary, these loss spikes share a common manifestation: abnormally large gradients are incorporated into the optimizer’s moment estimates, leading to unstable updates. Based on these analyses, we propose a unified remedy: **regardless of the root cause, instability in large-scale training is best addressed via gradient-centric clipping**. Specifically, only localized and adaptive clipping, applied *before* gradients are integrated into the optimizer’s moment estimates, can effectively constrain the influence of outlier gradients. We thus distill two key principles for loss spike mitigation: (1) *Locality*: clip gradients for each parameter tensor individually, avoiding the insensitivity of a global threshold; (2) *Adaptivity*: dynamically adjust each tensor’s clipping threshold, e.g., using an EMA of its recent gradient norms.

4. Methodology: AdaGC

4.1. Preliminaries

Notations. Let $x_t \in \mathbb{R}^d$ denote a parameter vector where x_t^j represents its j -th coordinate for $j \in [d]$. We write $\nabla_x f(x)$ for the gradient of any differentiable function $f : \mathbb{R}^d \rightarrow \mathbb{R}$, and use u^2 and u/v to denote element-wise square and division operations for vectors $u, v \in \mathbb{R}^d$. The ℓ_2 -norm and ℓ_{∞} -norm are denoted by $\|\cdot\|$ and $\|\cdot\|_{\infty}$, respectively. For asymptotic comparisons, we write $f = \mathcal{O}(g)$ if $\exists c > 0$ such that $f(x) \leq cg(x)$ for all x in the domain.

Gradient Clipping Fundamentals. Consider a stochastic optimization problem with parameters $\theta \in \mathbb{R}^d$ and loss function $f(\theta; X_t)$ evaluated on mini-batch X_t at step t . Standard gradient descent updates follow:

$$\theta_t = \theta_{t-1} - \eta_t \nabla_{\theta} f(\theta_{t-1}, X_t) \tag{1}$$

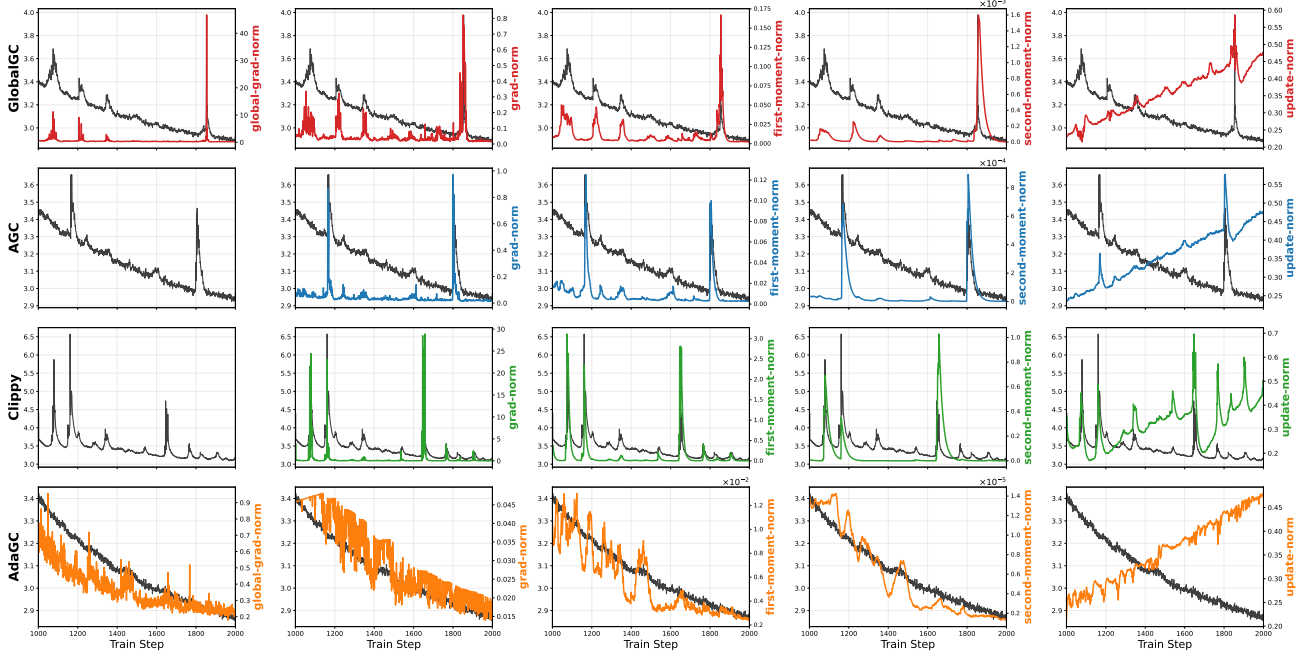


Figure 2. Visualization of the gradient norm, first-moment norm, second-moment norm, update norm, loss, and global gradient norm for the embedding of Llama-2 1.3B during warmup phase. Each row represents a different clipping method: the first row is GlobalGC, the second is AGC, the third is Clippy, and the fourth is our AdaGC. The black curve in each plot shows the loss trajectory.

To prevent unstable updates from gradient explosions, GlobalGC (Pascanu et al., 2013) modifies the update rule as:

$$\begin{aligned} \theta_t &= \theta_{t-1} - \eta_t h_t \nabla_{\theta} f(\theta_{t-1}, X_t) \\ \text{where } h_t &:= \min \left\{ \frac{\lambda_{abs}}{\|\nabla_{\theta} f(\theta_{t-1}; X_t)\|}, 1.0 \right\} \end{aligned} \quad (2)$$

Here λ_{abs} is an absolute clipping threshold requiring careful tuning, and η_t is the learning rate. Our work focuses on *norm-based* clipping (scaling entire gradients exceeding λ_{abs}) rather than *value-based* clipping (element-wise truncation).

4.2. Adaptive Gradient Clipping based on Local Gradient Norm

This section introduces a novel gradient clipping strategy termed AdaGC, which distinguishes itself by not relying on a global gradient norm. Instead, AdaGC focuses on the local gradient norm of each tensor and utilizes a dynamic adaptive mechanism for gradient clipping. The proposed method employs an EMA mechanism to maintain smoothed estimates of historical gradient norms per tensor, thus enhancing the accuracy of anomalous gradient detection and enabling independent clipping adjustments tailored to each tensor’s specific conditions. EMA is widely used in deep learning, and within AdaGC, it facilitates the balancing of historical and current gradient norms. The formulation is as follows:

$$\begin{aligned} \mathbf{g}_{t,i} &\leftarrow h_{t,i} \cdot \mathbf{g}_{t,i}, \text{ where } h_{t,i} = \min \left\{ \lambda_{rel} \frac{\gamma_{t-1,i}}{\|\mathbf{g}_{t,i}\|}, 1.0 \right\}, \\ \gamma_{t,i} &= \beta \gamma_{t-1,i} + (1 - \beta) \|\mathbf{g}_{t,i}\|. \end{aligned} \quad (3)$$

Here, λ_{rel} is a predefined relative clipping threshold, $\mathbf{g}_{t,i}$ represents the gradient of the i -th tensor at time step t , and $h_{t,i}$ is a clipping function activated when $\|\mathbf{g}_{t,i}\| > \lambda_{rel} \cdot \gamma_{t-1,i}$, thereby scaling the gradient norm to $\lambda_{rel} \cdot \gamma_{t-1,i}$. Additionally, β is the smoothing coefficient for EMA. We consistently incorporate the clipped gradient norm into the historical observations rather than the pre-clipped values.

Despite its simplicity, AdaGC adaptively adjusts based on the magnitude of each tensor’s gradient norm. Whenever the gradient norm at a current timestep exceeds a predefined range of average norms within a historical window, it effectively suppresses these outlier gradients.

However, during the initial stages of model training (e.g., the first 100 steps), the gradient norms are typically large and fluctuate significantly, indicating a substantial decreasing trend. Direct application of AdaGC during this period could lead to two issues: first, erroneously accumulating the early large gradient norms into the historical values, resulting in compounded errors; second, compared to GlobalGC, AdaGC might delay clipping, thus potentially slowing down the loss reduction. To address these issues, we introduce a hyperparameter T_{start} (default set to 100), representing a warm-up period during which traditional GlobalGC is applied.

Additionally, AdaGC is optimizer-agnostic, can be seamlessly integrated with various optimizers, such as AdamW (Loshchilov & Hutter, 2017), Lion (Chen et al., 2024), Muon (Jordan et al., 2024), enhancing its practicality

and flexibility. Algorithm 1 in Appendix A demonstrates its implementation with the AdamW optimizer.

4.3. Memory, Computation, and Communication

Memory. As a tensor-wise method, AdaGC maintains an EMA of gradient norms for each parameter tensor, requiring storage of a single 32-bit float (4 bytes) per tensor. For ERNIE models, the total additional memory overhead has complexity of $\mathcal{O}((9 + 3E) \times L + 3)$, where L and E denote the number of transformer layers and experts, respectively. Specifically, this includes four tensors from the attention module per layer, $3 \times (1 + E)$ tensors from the shared and router experts per layer, and two RMSNorm tensors per layer; plus one tensor each for the embedding layer, the final layer normalization, and the language modeling head. In practice, this added memory footprint is negligible compared to the overall memory requirements of large-scale model training.

Computation. The computational cost of computing ℓ_2 norms is the same for both AdaGC and GlobalGC. The difference is that GlobalGC applies a uniform scaling to all gradients, while AdaGC scales each gradient tensor independently.

Communication. In setups involving data parallelism (DP), tensor parallelism (TP), and pipeline parallelism (PP), GlobalGC requires an all-reduce operation across all DP, TP, and PP groups to aggregate the global norm. In contrast, AdaGC only needs an all-reduce within each TP group to compute per-tensor local norms. This design substantially reduces communication overhead, offering increasing benefits as model and cluster sizes grow.

5. Experiments

5.1. Experimental Setup

Models and Datasets. AdaGC is designed to enhance training stability during large language model pretraining. We evaluate its effectiveness on both dense and MoE (Mixture-of-Experts) architectures. For dense models, we use Llama-2 with 1.3B and 7B parameters. For MoE models, we experiment with Mixtral $8 \times 1B$ (Jiang et al., 2024) and ERNIE 10B-A1.4B (Baidu-ERNIE-Team, 2025), where Mixtral $8 \times 1B$ is a scaled-down version of Mixtral $8 \times 7B$, and ERNIE 10B-A1.4B is derived from ERNIE-4.5 21B-A3B. For pre-training, we use C4-en (Raffel et al., 2020), a clean English text corpus extracted from Common Crawl.

Comparison Methods. We focus on *clipping-based* methods and compare gradient and update clipping baselines, including GlobalGC (Pascanu et al., 2013), Gradient Value Clipping (ClipByValue), AGC (Brock et al., 2021), and Clippy (Tang et al., 2023). We also evaluate recent meth-

ods, including SPAM (Huang et al., 2025), Scaled Embed (Takase et al., 2023), and WeSaR (Nishida et al., 2024). Results are in Appendix D.2 Table 12.

Training Details. Pre-training large-scale models is typically resource-intensive. In this study, our primary focus was to investigate training instability rather than to pursue ultimate accuracy. To facilitate multiple experimental runs, we conducted 9,000 training steps over 36 billion tokens for both Llama-2 1.3B and 7B, 36,000 steps over 36 billion tokens for Mixtral $8 \times 1B$, and 60,000 steps over 1 trillion tokens for ERNIE 10B-A1.4B, the latter additionally serving to validate the long-term stability of AdaGC. Further details regarding hyperparameters can be found in Table 9 in Appendix B.

Evaluation Metrics. To quantitatively assess training stability, we follow (OLMo et al., 2024; Karpathy, 2024) and adopt the *spike score* as an objective metric. Specifically, the spike score is defined as the percentage of values in a time series that deviate by at least ten standard deviations from a rolling average of the preceding 1,000 values. This metric is primarily applied to training loss to detect sudden instabilities. Additionally, we evaluate performance using the training loss and validation perplexity (PPL) curves, as well as standard benchmark results, to provide a comprehensive assessment of convergence efficiency and model quality.

Standard Benchmark. We conducted a comprehensive evaluation of the model’s zero-shot and two-shot capabilities across seven well-established benchmarks: ARC (Yadav et al., 2019), BoolQ (Clark et al., 2019), HellaSwag (Zellers et al., 2019), OBQA (Mihaylov et al., 2018), PIQA (Bisk et al., 2020), WinoGrande (Sakaguchi et al., 2021), and MMLU (Hendrycks et al., 2020). Following standard practice (Zhang et al., 2025), we report accuracy norm for ARC-E, ARC-C, HellaSwag, OBQA, and SciQ, as well as standard accuracy for all other tasks. For ERNIE 10B-A1.4B, which has been trained on 1T tokens, we evaluate its general abilities on a range of benchmarks, including MMLU (Hendrycks et al., 2020), GSM8K (Cobbe et al., 2021), BBH (Suzgun et al., 2022), TruthfulQA (Lin et al., 2021), and HumanEval (Chen et al., 2021). These benchmarks assess the model’s enhanced capabilities in performing diverse downstream tasks, such as examination, reasoning, factuality, and coding.

5.2. Critical Hyperparameter Selection

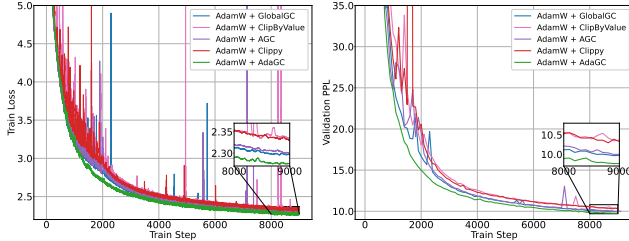
We systematically evaluated two key hyperparameters in AdaGC: the EMA coefficient β and the relative clipping threshold λ_{rel} . Specifically, we performed a grid search on the Llama-2 7B model to optimize these two hyperparameters, using zero-shot and two-shot performance across multiple tasks as evaluation metrics. As shown in Tables 3 and 4,

Table 3. Zero-shot accuracy of AdaGC on Llama-2 7B under different hyperparameters.

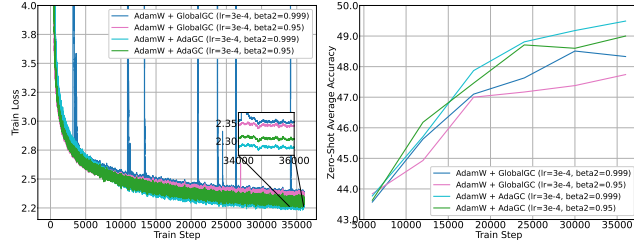
$\lambda_{rel} \backslash \beta$	0.98	0.985	0.99	0.999
1.03	50.06	50.92	50.95	50.96
1.04	48.88	50.59	51.04	50.76
1.05	<u>51.01</u>	49.95	50.57	50.74

Table 4. Two-shot accuracy of AdaGC on Llama-2 7B under different hyperparameters.

$\lambda_{rel} \backslash \beta$	0.98	0.985	0.99	0.999
1.03	52.31	52.68	53.13	53.42
1.04	52.68	53.01	<u>53.47</u>	52.85
1.05	52.68	52.67	51.96	53.51



(a) Llama-2 7B training dynamics.



(b) Mixtral 8x1B training dynamics.

Figure 3. Large language model training analysis: Llama-2 7B and Mixtral 8x1B model comparison shows AdaGC’s loss spike elimination and performance gains.

the best performance was achieved when $\lambda_{rel} = 1.04$ and $\beta = 0.99$. We therefore adopted this configuration as the default setting for subsequent experiments and terminated further hyperparameter search. In addition, as observed in Tables 3 and 4, AdaGC’s performance remains relatively stable across different hyperparameter values, suggesting that the method is robust to hyperparameter variations.

5.3. Main Experimental Results

Training Stability. Our comprehensive evaluation shows AdaGC’s effectiveness in improving training stability across a range of model scales and architectures. As shown in Figure 3, we compare the training dynamics of Llama-2 7B and Mixtral 8x1B models in terms of loss trajectories, validation perplexity, and zero-shot average accuracy. For the 7B models, baseline methods (GlobalGC, ClipByValue, AGC, Clippy) consistently exhibit frequent loss spikes during training, while AdaGC effectively eliminates these instability events. On Mixtral 8x1B, using the default $\beta_2 = 0.999$ leads to recurrent loss spikes, whereas decreasing β_2 to 0.95 helps mitigate this issue, indicating the strong impact of β_2 on training stability. AdaGC, however, can eliminate loss spikes for both $\beta_2 = 0.999$ and $\beta_2 = 0.95$, further demonstrating its robustness. The zero-shot average accuracy curves also reveal that AdaGC not only stabilizes training under $\beta_2 = 0.999$, but also improves convergence performance. For the ERNIE 10B-A1.4B, Figure 1b shows that stable convergence is achieved with $\epsilon = 1e-15$, which is particularly advantageous for large-scale models as it enables more parameters to fully utilize the adaptive learning rate in AdamW. Furthermore, Figure 2 illustrates AdaGC’s clipping process, which prevents abnormal gradients from entering optimizer states, further smoothing parameter updates and reducing oscillations, thereby benefiting training stability.

Spike Score Analysis. Table 7 quantitatively summarizes the reduction in spike score achieved by AdaGC and the baseline methods across various settings. For Llama-2 7B, the spike score is reduced from 0.0333 with GlobalGC to 0 with AdaGC; for Mixtral 8x1B, it drops from 0.0144 to 0; and for ERNIE 10B-A1.4B, from 0.01 to 0. These results consistently demonstrate that AdaGC effectively and robustly eliminates loss spikes compared to existing clipping methods.

Results on Downstream Benchmarks. Downstream zero-shot and two-shot evaluation results on the Llama-2 1.3B/7B and Mixtral 8x1B models (see Table 5 and Table 11) clearly demonstrate the practical benefits of stable training. Across all model scales, AdaGC consistently achieves state-of-the-art performance or matches the best baselines. Specifically, on Llama-2 7B and Mixtral 8x1B, AdaGC obtains superior zero-shot (51.01% / 49.01%) and two-shot (53.47% / 51.61%) average accuracy, surpassing the GlobalGC baseline by +1.32% / +1.27% and +0.83% / +1.14%, respectively. Furthermore, long-term training of ERNIE 10B-A1.4B on 350B tokens shows that AdaGC achieves more stable convergence with $\epsilon = 1e-15$, resulting in a 2.48% improvement over GlobalGC on the general abilities validation set. These findings establish a strong correlation between training stability and final model quality, indicating that the stability enabled by AdaGC facilitates better convergence and enhanced downstream performance.

5.4. Optimizer Compatibility: Muon and Lion

AdaGC is an optimizer-agnostic gradient clipping method that can be seamlessly integrated not only with AdamW, but also with other optimizers. To verify the generality of AdaGC, we conducted experiments on both LLM and VLM tasks by combining Llama-2 1.3B and CLIP ViT-Base mod-

AdaGC: Enhancing LLM Pretraining Stability via Adaptive Gradient Clipping

Table 5. The Zero-Shot evaluation results of Llama-2 1.3B/7B and Mixtral 8x1B models on standard benchmarks.

Model	Method	ARC-E acc_norm	ARC-C acc_norm	BoolQ acc	HellaSw. acc_norm	OBQA acc_norm	PIQA acc_norm	W.G. acc	MMLU acc	SciQ acc_norm	Avg.
Llama-2 1.3B	GlobalGC	43.18	25.68	57.19	46.62	30.20	69.97	52.64	22.97	68.40	46.32
	ClipByValue	42.17	25.68	59.94	44.11	30.40	69.59	53.28	22.99	68.00	46.24
	Clippy	41.71	24.66	56.51	45.43	30.00	69.21	54.85	22.90	67.50	45.86
	AdaGC	42.09	25.51	58.01	47.29	30.40	69.70	52.33	22.98	68.70	46.33
Llama-2 7B	GlobalGC	49.49	27.56	56.30	56.06	33.60	74.59	55.33	23.12	71.20	49.69
	ClipByValue	46.21	26.88	57.03	53.49	33.20	71.65	53.59	23.36	70.50	48.43
	AGC	48.15	28.16	52.87	55.47	32.80	72.74	57.85	24.33	71.70	49.34
	Clippy	47.69	27.73	57.46	53.34	32.40	72.74	54.38	25.36	73.40	49.39
	AdaGC	49.58	28.92	57.28	57.94	32.80	74.32	58.09	23.62	76.60	51.01
Mixtral 8x1B	GlobalGC	44.70	25.94	56.57	53.08	33.00	71.60	54.70	22.91	67.20	47.74
	AdaGC	46.68	26.37	58.93	55.85	32.20	73.12	54.38	23.22	70.30	49.01

Table 6. Evaluation results of ERNIE 10B-A1.4B on multiple benchmarks after 21,000 (350B tokens) and 60,000 (1T tokens) training steps, comparing different optimization configurations.

Steps (tokens)	Method	AdamW eps	MMLU	GSM8K	BBH	TruthfulQA	HumanEval	Avg.
21k (350B)	GlobalGC	1e-8	47.75	28.35	28.80	22.02	19.51	28.09
	GlobalGC	1e-15	39.11	21.46	29.35	23.39	15.24	25.71
	AdaGC	1e-15	42.07	25.32	27.89	24.92	20.73	28.19
60k (1T)	GlobalGC	1e-8	48.61	39.88	30.84	30.73	22.56	34.52
	GlobalGC	1e-15	48.48	40.79	30.59	28.29	23.78	34.38
	AdaGC	1e-15	48.70	36.01	31.38	35.02	22.56	34.73

Table 7. Comparison of spike scores for various models under different clipping methods.

Model	Llama-2 7B					Mixtral 8x1B		ERNIE 10B-A1.4B	
	GlobalGC	ClipByValue	AGC	Clippy	AdaGC	GlobalGC	AdaGC	GlobalGC	AdaGC
Total Steps	9K	9K	9K	9K	9K	36K	36K	21K	21K
Num Spikes	3	9	8	3	0	52	0	2	0
Spike Score (%)	0.0333	0.1000	0.0889	0.0333	0.0000	0.0144	0.0000	0.0100	0.0000

Table 8. GPU hours under the same configuration. DPS denotes distributed parallel strategies.

Model	Llama-2 1.3B	Llama-2 7B	Mixtral 8x1B	ERNIE 10B-A1.4B
DPS	DP=256, TP=1, PP=1	DP=32, TP=2, PP=1	DP=256, TP=1, PP=1, EP=1	DP=64, TP=1, PP=4, EP=8
Steps	9K	9K	36K	21K
GlobalGC	513.0	1468.2	2060.8	22922
AdaGC	511.6	1402.4	2035.2	22572

els with the Muon and Lion optimizers, respectively, and compared them against GlobalGC. Although no loss spikes were observed under either experimental setting, AdaGC consistently demonstrated strong compatibility and generalization. In downstream zero-shot average accuracy, AdaGC outperformed GlobalGC by 0.14% (47.18% vs. 47.04%) with Muon and by 0.16% (40.81% vs. 40.65%) with Lion. These results further confirm that AdaGC can be effectively applied across different optimizers, providing stable training and improved downstream performance.

5.5. End-to-End training Wall-clock

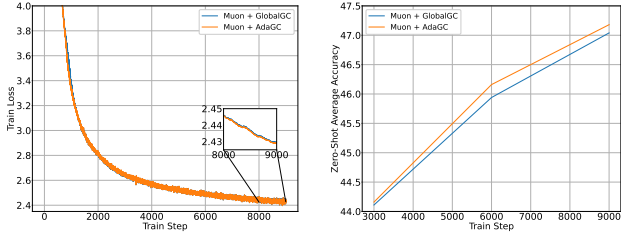
Table 8 compares the GPU hours required for training various models using different distributed parallelism strategies. Compared to GlobalGC, AdaGC reduces end-to-end GPU hours by 0.27% on Llama-2 1.3B, 4.48% on Llama-2 7B, 1.24% on Mixtral 8x1B, and 1.53% on ERNIE 10B-A1.4B,

thanks to reduced communication overhead. This highlights AdaGC’s additional communication and efficiency benefits in large-scale distributed training.

5.6. Ablation Study

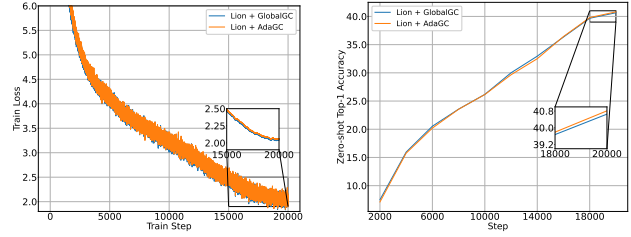
We conduct systematic ablation studies across three critical dimensions of AdaGC: (1) EMA gradient norm initialization strategies, (2) GlobalGC warm-up steps, (3) adaptivity efficacy, and (4) locality granularity.

EMA Initialization Strategy. The initialization of EMA gradient norms requires careful design due to large initial gradient fluctuations during early training phases (first 100 steps). We evaluate five initialization variants: The default AdaGC strategy employs GlobalGC during warm-up while tracking minimum per-parameter norms ($\gamma_{t,i} = \min(\|g_{t,i}\|, \gamma_{t-1,i})$). Comparative approaches include: (1) norm initialization without GlobalGC warm-up (directly



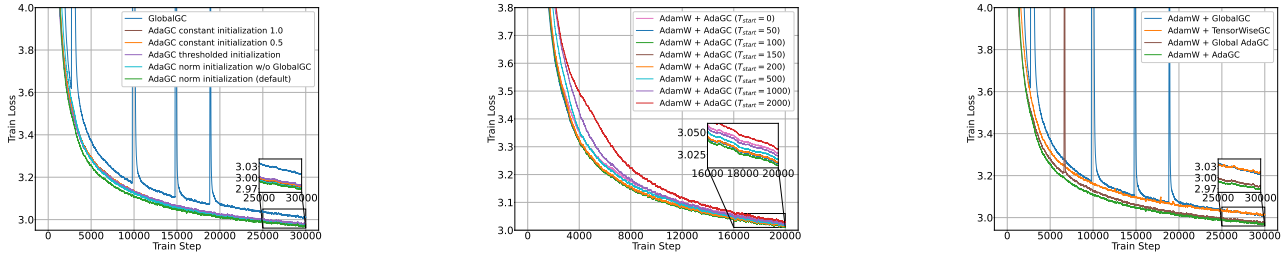
(a) Training dynamics. (b) Average accuracy.

Figure 4. AdaGC with Muon on Llama-2 1.3B.



(a) Training dynamics. (b) Average accuracy.

Figure 5. AdaGC with Lion on CLIP ViT-Base.



(a) $\gamma_{t,i}$ initialization. (b) T_{start} warm-up. (c) Adaptivity, locality.

Figure 6. Training dynamics of AdaGC ablations, showing (a) the influence of different EMA initialization strategies; (b) the impact of the GlobalGC warm-up steps T_{start} ; and (c) the effects of adaptivity and locality granularity on gradient clipping efficacy and final loss.

using $\gamma_{t,i} = \min(\|\mathbf{g}_{t,i}\|, \gamma_{t-1,i})$ from step 0), (2) constant initialization ($\gamma_{0,i} \in \{0.5, 1.0\}$), and (3) thresholded initialization ($\gamma_{t,i} = \min(\|\mathbf{g}_{t,i}\|, 0.1)$). Figure 6a demonstrates that while all variants eliminate loss spikes, convergence quality varies within 0.36%. The default strategy achieves optimal final loss (2.9708 vs 2.9725 for next-best), showing that GlobalGC-guided warm-up better preserves parameter update consistency than direct initialization. This establishes the importance of phased initialization for gradient norm adaptation.

Warm-up Steps T_{start} . To further investigate whether the choice of GlobalGC warm-up steps T_{start} has a significant impact and to provide practical guidance for practitioners, we additionally evaluate $T_{start} = \{0, 50, 100, 150, 200, 500, 1000, 2000\}$. The results in Figure 6b show that $T_{start} = 100$ consistently achieves the best performance. According to the EMA initialization formula $\gamma_{t,i} = \min(\|\mathbf{g}_{t,i}\|, \gamma_{t-1,i})$, an excessively large T_{start} accumulates lower $\gamma_{t,i}$ values due to early training dynamics, which may lead to over-clipping and suppressed convergence in later training. Conversely, an overly small T_{start} accumulates larger $\gamma_{t,i}$ values, which may delay clipping and hinder timely suppression of abnormal gradients. In contrast, $T_{start} = 100$ introduces negligible additional overhead for large-scale training while providing consistently stable performance improvements.

Adaptivity Efficacy and Locality Granularity. We conduct three sets of ablation experiments to evaluate the adaptivity and locality of AdaGC. The baseline uses GlobalGC (no adaptivity, no locality) with a fixed threshold of 1.0. In comparison, we examine (1) adaptive global gradient norm clipping (Global AdaGC, adaptive but non-local), which

employs a single adaptive threshold for the entire model, (2) tensor-wise gradient norm clipping (TensorWiseGC, local but non-adaptive), which allocated each tensor’s fixed clipping threshold proportionally to its parameter count relative to the entire model, and (3) tensor-wise adaptation (AdaGC, adaptive and local), which adjusts thresholds independently for each tensor. As shown in Figure 6c, Global AdaGC reduces but does not completely eliminate spike events (1 event vs. 0 for tensor-wise) and yields a 0.25% higher final loss (2.9639 vs. 2.9712). Although TensorWiseGC also mitigates loss spikes, it noticeably slows down convergence and requires careful per-tensor threshold tuning to perform well. These results demonstrate that tensor-wise adaptive clipping provides both greater spike suppression and lower loss than other approaches.

6. Conclusion

The factors triggering loss spikes in large-scale pretraining are diverse and remain an open research problem, with no unified solution to date. Unlike prior work that seeks to identify root causes, we focus on a gradient-centric remedy and introduce AdaGC, an adaptive per-tensor gradient clipping method that prevents abnormal gradients from contaminating optimizer states. This approach ensures smoother updates and effectively eliminates loss spikes. Extensive experiments demonstrate that AdaGC delivers robust and stable training across both dense and MoE models, from 1.3B to 10B parameters, consistently reducing spike scores to zero and improving benchmark performance. Our results highlight AdaGC as a simple and effective solution for stable large-scale model pretraining.

Impact Statement

This paper presents work whose goal is to advance the field of Machine Learning. There are many potential societal consequences of our work, none which we feel must be specifically highlighted here.

References

- Bai, Z., Zhou, Z., Zhao, J., Li, X., Li, Z., Xiong, F., Yang, H., Zhang, Y., and Xu, Z.-Q. J. Adaptive preconditioners trigger loss spikes in adam. *arXiv preprint arXiv:2506.04805*, 2025.
- Baidu-ERNIE-Team. Ernie 4.5 technical report, 2025.
- Bisk, Y., Zellers, R., Gao, J., Choi, Y., et al. Piqa: Reasoning about physical commonsense in natural language. In *Proceedings of the AAAI conference on artificial intelligence*, volume 34, pp. 7432–7439, 2020.
- Brock, A., De, S., Smith, S. L., and Simonyan, K. High-performance large-scale image recognition without normalization. In *International Conference on Machine Learning*, pp. 1059–1071. PMLR, 2021.
- Cattaneo, M. D. and Shigida, B. Tuning Adam(W): Default β_2 may be too large. Working paper, Princeton University, 2025. URL https://github.com/mdcattaneo/mdcattaneo.github.io/blob/ca84a9d43db12951e75190ae76fbdaabc77133f0/papers/Cattaneo-Shigida_2025_TuningAdam.pdf.
- Chen, M., Tworek, J., Jun, H., Yuan, Q., Pinto, H. P. D. O., Kaplan, J., Edwards, H., Burda, Y., Joseph, N., Brockman, G., et al. Evaluating large language models trained on code. *arXiv preprint arXiv:2107.03374*, 2021.
- Chen, X., Liang, C., Huang, D., Real, E., Wang, K., Pham, H., Dong, X., Luong, T., Hsieh, C.-J., Lu, Y., et al. Symbolic discovery of optimization algorithms. *Advances in Neural Information Processing Systems*, 36, 2024.
- Chowdhery, A., Narang, S., Devlin, J., Bosma, M., Mishra, G., Roberts, A., Barham, P., Chung, H. W., Sutton, C., Gehrmann, S., et al. Palm: Scaling language modeling with pathways. *Journal of Machine Learning Research*, 24(240):1–113, 2023.
- Clark, C., Lee, K., Chang, M.-W., Kwiatkowski, T., Collins, M., and Toutanova, K. Boolq: Exploring the surprising difficulty of natural yes/no questions. *arXiv preprint arXiv:1905.10044*, 2019.
- Cobbe, K., Kosaraju, V., Bavarian, M., Chen, M., Jun, H., Kaiser, L., Plappert, M., Tworek, J., Hilton, J., Nakano, R., et al. Training verifiers to solve math word problems. *arXiv preprint arXiv:2110.14168*, 2021.
- Dao, T. Flashattention-2: Faster attention with better parallelism and work partitioning. *arXiv preprint arXiv:2307.08691*, 2023.
- Goyal, P., Dollár, P., Girshick, R., Noordhuis, P., Wesolowski, L., Kyrola, A., Tulloch, A., Jia, Y., and He, K. Accurate, large minibatch sgd: Training imagenet in 1 hour. *arXiv preprint arXiv:1706.02677*, 2017.
- Han, D. Gemma bug fixes - approx gelu, layernorms, sqrt(hd), Mar 2024. URL <https://github.com/huggingface/transformers/pull/29402>. GitHub Pull Request #29402, huggingface/transformers.
- Hendrycks, D., Burns, C., Basart, S., Zou, A., Mazeika, M., Song, D., and Steinhardt, J. Measuring massive multitask language understanding. *arXiv preprint arXiv:2009.03300*, 2020.
- Huang, T., Zhu, Z., Jin, G., Liu, L., Wang, Z., and Liu, S. Spam: Spike-aware adam with momentum reset for stable llm training. *arXiv preprint arXiv:2501.06842*, 2025.
- Jiang, A. Q., Sablayrolles, A., Roux, A., Mensch, A., Savary, B., Bamford, C., Chaplot, D. S., Casas, D. d. l., Hanna, E. B., Bressand, F., et al. Mixtral of experts. *arXiv preprint arXiv:2401.04088*, 2024.
- Jordan, K., Jin, Y., Boza, V., You, J., Cesista, F., Newhouse, L., and Bernstein, J. Muon: An optimizer for hidden layers in neural networks, 2024. URL <https://kellerjordan.github.io/posts/muon/>.
- Karpathy, A. Cool! for the spike i’d try e.g. ‘-sl 7 -sg 7’ to keep instability in check earlier in the training. (will skip update if loss/gradnorm > 7 sigma outlier is detected). X (formerly Twitter), July 2024. <https://x.com/karpathy/status/1812917107379872145>.
- Kingma, D. P. and Ba, J. Adam: A method for stochastic optimization. *arXiv preprint arXiv:1412.6980*, 2014.
- Li, Y., Fan, H., Hu, R., Feichtenhofer, C., and He, K. Scaling language-image pre-training via masking. In *Proceedings of the IEEE/CVF Conference on Computer Vision and Pattern Recognition*, pp. 23390–23400, 2023.
- Lin, S., Hilton, J., and Evans, O. Truthfulqa: Measuring how models mimic human falsehoods. *arXiv preprint arXiv:2109.07958*, 2021.
- Liu, A., Feng, B., Xue, B., Wang, B., Wu, B., Lu, C., Zhao, C., Deng, C., Zhang, C., Ruan, C., et al. Deepseek-v3 technical report. *arXiv preprint arXiv:2412.19437*, 2024.
- Loshchilov, I. and Hutter, F. Sgdr: Stochastic gradient descent with warm restarts. *arXiv preprint arXiv:1608.03983*, 2016.

- Loshchilov, I. and Hutter, F. Decoupled weight decay regularization. *arXiv preprint arXiv:1711.05101*, 2017.
- Ma, C., Wu, L., and E, W. A qualitative study of the dynamic behavior for adaptive gradient algorithms, 2021. URL <https://arxiv.org/abs/2009.06125>.
- Mihaylov, T., Clark, P., Khot, T., and Sabharwal, A. Can a suit of armor conduct electricity? a new dataset for open book question answering. *arXiv preprint arXiv:1809.02789*, 2018.
- Nguyen, T. Q. and Salazar, J. Transformers without tears: Improving the normalization of self-attention. *arXiv preprint arXiv:1910.05895*, 2019.
- Nishida, K., Nishida, K., and Saito, K. Initialization of large language models via reparameterization to mitigate loss spikes. *arXiv preprint arXiv:2410.05052*, 2024.
- OLMo, T., Walsh, P., Soldaini, L., Groeneveld, D., Lo, K., Arora, S., Bhagia, A., Gu, Y., Huang, S., Jordan, M., et al. 2 olmo 2 furious. *arXiv preprint arXiv:2501.00656*, 2024.
- Pascanu, R., Mikolov, T., and Bengio, Y. On the difficulty of training recurrent neural networks. In *International conference on machine learning*, pp. 1310–1318. Pmlr, 2013.
- Radford, A., Kim, J. W., Hallacy, C., Ramesh, A., Goh, G., Agarwal, S., Sastry, G., Askell, A., Mishkin, P., Clark, J., et al. Learning transferable visual models from natural language supervision. In *International conference on machine learning*, pp. 8748–8763. PMLR, 2021.
- Raffel, C., Shazeer, N., Roberts, A., Lee, K., Narang, S., Matena, M., Zhou, Y., Li, W., and Liu, P. J. Exploring the limits of transfer learning with a unified text-to-text transformer. *Journal of machine learning research*, 21 (140):1–67, 2020.
- Reddi, S. J., Kale, S., and Kumar, S. On the convergence of adam and beyond. In *International Conference on Learning Representations*, 2018.
- Russakovsky, O., Deng, J., Su, H., Krause, J., Satheesh, S., Ma, S., Huang, Z., Karpathy, A., Khosla, A., Bernstein, M., et al. Imagenet large scale visual recognition challenge. *International journal of computer vision*, 115: 211–252, 2015.
- Sakaguchi, K., Bras, R. L., Bhagavatula, C., and Choi, Y. Winogrande: An adversarial winograd schema challenge at scale. *Communications of the ACM*, 64(9):99–106, 2021.
- Schuhmann, C., Vencu, R., Beaumont, R., Kaczmarczyk, R., Mullis, C., Katta, A., Coombes, T., Jitsev, J., and Komatsuzaki, A. Laion-400m: Open dataset of clip-filtered 400 million image-text pairs. *arXiv preprint arXiv:2111.02114*, 2021.
- Shazeer, N. and Stern, M. Adafactor: Adaptive learning rates with sublinear memory cost. In *International Conference on Machine Learning*, pp. 4596–4604. PMLR, 2018.
- Su, J. Why is the default norm for gradient clipping 1?, Jan 2025. URL <https://spaces.ac.cn/archives/10657>.
- Suzgun, M., Scales, N., Schärli, N., Gehrmann, S., Tay, Y., Chung, H. W., Chowdhery, A., Le, Q. V., Chi, E. H., Zhou, D., et al. Challenging big-bench tasks and whether chain-of-thought can solve them. *arXiv preprint arXiv:2210.09261*, 2022.
- Takase, S., Kiyono, S., Kobayashi, S., and Suzuki, J. Spike no more: Stabilizing the pre-training of large language models. *arXiv preprint arXiv:2312.16903*, 2023.
- Tang, J., Drori, Y., Chang, D., Sathiamoorthy, M., Gilmer, J., Wei, L., Yi, X., Hong, L., and Chi, E. H. Improving training stability for multitask ranking models in recommender systems. In *Proceedings of the 29th ACM SIGKDD Conference on Knowledge Discovery and Data Mining*, pp. 4882–4893, 2023.
- Team, K., Bai, Y., Bao, Y., Chen, G., Chen, J., Chen, N., Chen, R., Chen, Y., Chen, Y., Chen, Y., et al. Kimi k2: Open agentic intelligence. *arXiv preprint arXiv:2507.20534*, 2025.
- Touvron, H., Lavril, T., Izacard, G., Martinet, X., Lachaux, M.-A., Lacroix, T., Rozière, B., Goyal, N., Hambro, E., Azhar, F., et al. Llama: Open and efficient foundation language models. *arXiv preprint arXiv:2302.13971*, 2023.
- Wortsman, M., Dettmers, T., Zettlemoyer, L., Morcos, A., Farhadi, A., and Schmidt, L. Stable and low-precision training for large-scale vision-language models. *Advances in Neural Information Processing Systems*, 36: 10271–10298, 2023.
- Xiong, R., Yang, Y., He, D., Zheng, K., Zheng, S., Xing, C., Zhang, H., Lan, Y., Wang, L., and Liu, T. On layer normalization in the transformer architecture. In *International Conference on Machine Learning*, pp. 10524–10533. PMLR, 2020.
- Yadav, V., Bethard, S., and Surdeanu, M. Quick and (not so) dirty: Unsupervised selection of justification sentences for multi-hop question answering. *arXiv preprint arXiv:1911.07176*, 2019.

Yang, A., Xiao, B., Wang, B., Zhang, B., Bian, C., Yin, C., Lv, C., Pan, D., Wang, D., Yan, D., et al. Baichuan 2: Open large-scale language models. *arXiv preprint arXiv:2309.10305*, 2023.

You, Y., Li, J., Reddi, S., Hseu, J., Kumar, S., Bhojanapalli, S., Song, X., Demmel, J., Keutzer, K., and Hsieh, C.-J. Large batch optimization for deep learning: Training bert in 76 minutes. *arXiv preprint arXiv:1904.00962*, 2019.

Zellers, R., Holtzman, A., Bisk, Y., Farhadi, A., and Choi, Y. Hellaswag: Can a machine really finish your sentence? *arXiv preprint arXiv:1905.07830*, 2019.

Zhang, B. and Sennrich, R. Root mean square layer normalization. *Advances in Neural Information Processing Systems*, 32, 2019.

Zhang, Y., Liu, Y., Yuan, H., Qin, Z., Yuan, Y., Gu, Q., and Yao, A. C.-C. Tensor product attention is all you need. *arXiv preprint arXiv:2501.06425*, 2025.

Appendix Contents

A. Pseudocode of AdamW with AdaGC	13
B. Hyper-Parameters	13
B.1. Model Hyper-Parameters	13
B.2. Clipping Hyper-Parameters	13
C. Experimental Details for CLIP	14
D. More Evaluation Results	15
D.1. Results on Downstream Benchmarks	15
D.2. Results of Other Baseline Methods	15
E. More Visualization Results	16
E.1. Training Dynamics	16
E.2. Optimizer State Dynamics	16
F. Convergence Analysis and Proof	20

A. Pseudocode of AdamW with AdaGC

Algorithm 1 presents the pseudocode of AdamW integrated with AdaGC. For clearer exposition, we highlight different components according to their origins: **orange** indicates the procedures inherited from the original GlobalGC algorithm, while **blue** is used to denote the new contributions and modifications introduced by AdaGC. Specifically, the GlobalGC steps include the global gradient clipping implemented via the scaling factor and the use of the clipped gradient in subsequent moments. The AdaGC components mainly comprise adaptive per-parameter clipping, the initialization and update of the adaptive threshold $\gamma_{t,i}$, and the warm-up strategy governed by T_{start} .

Algorithm 1 AdamW with AdaGC

```

1: given:  $\{\eta_t\}_{t=1}^T, \lambda_w, \epsilon, \beta_1, \beta_2, \beta \in [0, 1], \lambda_{abs}, T_{start}$ 
2: initialize:  $\theta_0, m_0 \leftarrow 0, v_0 \leftarrow 0, t \leftarrow 0$ 
3: repeat
4:   compute  $\mathbf{g}_t = \nabla_{\theta} f_t(\theta_{t-1}, X_t)$ 
5:   if  $t < T_{start}$  then
6:      $h_t = \min \left\{ \frac{\lambda_{abs}}{\|\mathbf{g}_t\|}, 1.0 \right\}$ 
7:      $\widehat{\mathbf{g}}_t = h_t \cdot \mathbf{g}_t$ 
8:     for  $i \in |\theta|$  do
9:        $\gamma_{t,i} = \min \left\{ \gamma_{t-1,i}, \|\widehat{\mathbf{g}}_{t,i}\| \right\}, \gamma_{0,i} = \|\widehat{\mathbf{g}}_{1,i}\|$ 
10:    end for
11:  else
12:    for  $i \in |\theta|$  do
13:       $h_{t,i} = \min \left\{ \lambda_{rel} \frac{\gamma_{t-1,i}}{\|\mathbf{g}_{t,i}\|}, 1.0 \right\}$ 
14:       $\widehat{\mathbf{g}}_{t,i} = h_{t,i} \cdot \mathbf{g}_{t,i}$ 
15:       $\gamma_{t,i} = \beta \gamma_{t-1,i} + (1 - \beta) \|\widehat{\mathbf{g}}_{t,i}\|$ 
16:    end for
17:  end if
18:   $\mathbf{m}_t = \beta_1 \mathbf{m}_{t-1} + (1 - \beta_1) \widehat{\mathbf{g}}_t$ 
19:   $\mathbf{v}_t = \beta_2 \mathbf{v}_{t-1} + (1 - \beta_2) \widehat{\mathbf{g}}_t^2$ 
20:   $\widehat{\mathbf{m}}_t = \mathbf{m}_t / (1 - \beta_1^t), \widehat{\mathbf{v}}_t = \mathbf{v}_t / (1 - \beta_2^t)$ 
21:   $\theta_t = \theta_{t-1} - \eta_t \lambda_w \theta_{t-1} - \eta_t \widehat{\mathbf{m}}_t / (\sqrt{\widehat{\mathbf{v}}_t} + \epsilon)$ 
22: until  $\theta_t$  not converge

```

B. Hyper-Parameters

B.1. Model Hyper-Parameters

Table 9 summarizes the model hyper-parameters used for all experiments. For each model, we report the core architecture settings (such as number of layers, hidden dimension, attention heads, and feedforward dimension), MoE-related configurations, and main optimization hyper-parameters (including learning rate, warmup, weight decay, and Adam parameters). Clipping thresholds λ_{abs} , λ_{rel} , and momentum β are also listed, in correspondence with the techniques discussed in the main text. All experiments use a batch size and sequence length as shown, and we employ bfloat16 precision for most models except ERNIE, which uses float8. The symbol ‘-’ indicates settings not applicable to a specific architecture.

B.2. Clipping Hyper-Parameters

For other clipping methods, we primarily followed the recommended default settings from prior work, and performed limited tuning only when necessary to ensure a fair comparison.

Specifically:

- **GlobalGC:** We used the commonly adopted global clipping threshold $\lambda_{abs} = 1.0$ in large-scale pretraining.
- **ClipByValue:** Following the SPAM (Huang et al., 2025) setting, we set the clipping threshold to $\lambda_{abs} = 1e - 3$.
- **AGC:** We performed small-range tuning over $\lambda_{rel} \in \{1e - 2, 1e - 3, 1e - 4\}$ to find the best setting.

Table 9. Hyper-parameters used in our LLMs experiments. λ_{abs} represents the absolute global clipping threshold of GlobalGC. λ_{rel} and β represent the relative clipping threshold and the momentum of our AdaGC, respectively. The symbol ‘-’ indicates that the parameter is not applicable.

Model	Llama-2 1.3B	Llama-2 7B	ERNIE 10B-A1.4B	Mixtral 8x1B
Precision	bfloat16	bfloat16	float8	bfloat16
Num layers	24	32	25	24
Hidden dim size	2048	4096	2560	2048
FFN dim size	5461	11008	1024	5632
Num attention heads	32	32	20	32
Num key value heads	32	32	4	4
Attention bias	✗	✗	✗	✗
Num shared experts	-	-	1	0
Num router experts	-	-	48	8
Num experts per token	-	-	3	2
Sequence length	2048	2048	4096	2048
Batch size	2048	2048	4096	512
Iterations	9000	9000	21000	36000
Learning rate	3.0×10^{-4}	3.0×10^{-4}	3.0×10^{-4}	3.0×10^{-4}
LR decay	cosine	cosine	wsd	cosine
Warmup iterations	2000	2000	2000	500
Weight decay	0.1	0.1	0.1	0.1
Adam β_1	0.90	0.90	0.90	0.90
Adam β_2	0.95	0.95	0.95	0.999
λ_{abs}	1.0	1.0	1.0	1.0
λ_{rel}	1.04	1.04	1.04	1.04
β	0.99	0.99	0.99	0.99

- **Clippy**: We tuned over $\lambda_{abs} \in \{0.1, 0.3, 0.5\}$ and $\lambda_{rel} \in \{1e-2, 1e-3, 1e-4\}$ to select the optimal combination.
- **SPAM**: We adopted the default hyperparameters recommended for standard pretraining in the original paper, which were reported to perform well across diverse settings. Specifically, we set the interval to $\Delta T = 500$, the threshold to $\theta = 5000$, and the warmup steps to $N = 150$.

The final hyper-parameters used for other clipping methods are summarized in Table 10.

Table 10. Hyper-parameters for other clipping methods.

Method	Hyperparameters
GlobalGC	$\lambda_{abs} = 1.0$
ClipByValue	$\lambda_{abs} = 1e-3$
AGC	$\lambda_{rel} = 1e-3$
Clippy	$\lambda_{abs} = 0.5, \lambda_{rel} = 1e-2$
SPAM	$\Delta T = 500, \theta = 5000, N = 150$

C. Experimental Details for CLIP

To further investigate the optimizer compatibility of AdaGC, we evaluated its effect on large-scale vision-language model pre-training, focusing on the CLIP ViT-Base model (Radford et al., 2021) with the Lion optimizer (Chen et al., 2024). The model comprises 151 million parameters and is trained on the LAION-400M (Schuhmann et al., 2021) dataset. Training is conducted for 20,000 steps, covering 320M image-text pairs.

The key training hyper-parameters are as follows: a learning rate of 0.002, weight decay of 0.2, and batch size of 32,768.

We employ patch-dropout with a drop rate of 0.5 (Li et al., 2023), following recent best practices (Wortsman et al., 2023). The learning rate is linearly warmed up for the first 5,000 steps (Goyal et al., 2017), and subsequently decayed according to a cosine schedule (Loshchilov & Hutter, 2016).

Following pre-training, we report downstream zero-shot evaluation results on the ImageNet (Russakovsky et al., 2015) validation set. The results are shown in Figure 5 in the main text.

D. More Evaluation Results

D.1. Results on Downstream Benchmarks

The Two-Shot evaluation results of Llama-2 1.3B/7B and Mixtral 8x1B models on standard benchmarks are presented in Table 11.

Table 11. The Two-Shot evaluation results of Llama-2 1.3B/7B and Mixtral 8x1B models on standard benchmarks. The best scores in each column are **bolded**. HellaSw. = HellaSwag, W.G. = WinoGrande.

Model	Method	ARC-E acc_norm	ARC-C acc_norm	BoolQ acc	HellaSw. acc_norm	OBQA acc_norm	PIQA acc_norm	W.G. acc	MMLU acc	SciQ acc_norm	Avg.
Llama-2 1.3B	GlobalGC	47.26	25.60	50.31	46.44	32.20	69.64	52.33	25.07	77.80	47.41
	ClipByValue	47.10	25.77	56.54	43.97	30.00	68.88	52.96	26.09	77.20	47.61
	Clippy	46.55	25.85	49.76	45.71	30.00	70.02	53.20	25.69	77.70	47.16
	AdaGC	46.04	26.19	49.72	47.51	31.00	69.70	54.38	24.98	78.50	47.56
Llama-2 7B	GlobalGC	55.81	28.58	60.70	56.54	33.00	73.72	56.75	25.51	83.20	52.64
	ClipByValue	51.94	26.88	57.55	53.36	32.40	72.31	54.14	26.63	81.60	50.75
	AGC	52.95	28.67	56.15	55.69	35.40	73.07	56.43	26.88	82.80	52.00
	Clippy	52.86	29.10	56.48	53.76	31.80	73.07	55.72	26.03	82.60	51.27
	AdaGC	56.86	29.61	59.36	57.89	33.60	73.99	57.62	26.46	85.90	53.47
Mixtral 8x1B	GlobalGC	50.34	27.39	58.81	52.96	34.20	71.16	54.06	25.37	79.90	50.47
	AdaGC	53.83	28.42	58.69	55.66	33.80	73.07	54.14	25.12	81.80	51.61

D.2. Results of Other Baseline Methods

Table 12. The Zero-Shot evaluation results of Llama-2 1.3B/7B models on standard benchmarks.

Model	Method	ARC-E acc_norm	ARC-C acc_norm	BoolQ acc	HellaSw. acc_norm	OBQA acc_norm	PIQA acc_norm	W.G. acc	MMLU acc	SciQ acc_norm	Avg.
Llama-2 1.3B	WeSaR-GlobalGC	43.56	25.17	59.94	45.08	30.00	70.29	52.96	22.90	65.80	46.19
	SPAM	42.05	24.83	59.60	42.82	30.00	69.31	52.17	23.02	66.40	45.58
	ScaledEmbed-GlobalGC	42.21	25.51	59.66	45.50	31.80	70.02	53.28	23.22	65.20	46.27
	AdaGC	42.09	25.51	58.01	47.29	30.40	69.70	52.33	22.98	68.70	46.33
Llama-2 7B	WeSaR-GlobalGC	49.75	27.22	56.12	55.38	33.80	73.39	56.27	23.02	71.40	49.59
	SPAM	48.53	25.77	60.34	51.89	32.60	72.03	54.54	22.95	71.00	48.85
	ScaledEmbed-GlobalGC	48.57	26.71	60.89	54.32	32.60	72.25	55.33	23.66	70.50	49.42
	AdaGC	49.58	28.92	57.28	57.94	32.80	74.32	58.09	23.62	76.60	51.01

Table 13. Comparison of spike scores for various models under different methods.

Model	Llama-2 1.3B				Llama-2 7B			
	WeSaR-GlobalGC	SPAM	ScaledEmbed-GlobalGC	AdaGC	WeSaR-GlobalGC	SPAM	ScaledEmbed-GlobalGC	AdaGC
Total Steps	9K	9K	9K	9k	9K	9K	9K	9K
Num Spikes	2	0	10	0	1	3	8	0
Spike Score (%)	0.0222	0.0000	0.1111	0.0000	0.0111	0.0333	0.0889	0.0000

In addition to the clipping-based baselines discussed in the main text, we also compare AdaGC with several recent methods that aim to improve the stability and generalization of large language model (LLM) training, including SPAM (Huang et al., 2025), Scaled Embed (Takase et al., 2023), and WeSaR (Nishida et al., 2024). The detailed results under the zero-shot setting and spike score are summarized in Table 12 and 13. The training dynamics are shown in Figures 8 and 9.

Among these methods, SPAM is designed to stabilize training by adjusting the optimizer’s behavior, while Scaled Embed and WeSaR focus on initialization or embedding scaling strategies to suppress loss spikes. Our experiments show that, although some of these methods can partly mitigate instability or improve certain metrics, AdaGC generally achieves higher stability and better final performance across model scales. Notably, while WeSaR is also effective at suppressing loss spikes, its reliance on special parameter initialization limits its applicability to from-scratch training. In contrast, AdaGC works reliably under both from-scratch and resumed training regimes, providing stronger flexibility. Overall, these results demonstrate AdaGC’s superior robustness and generalization compared to other non-clipping baselines.

E. More Visualization Results

E.1. Training Dynamics

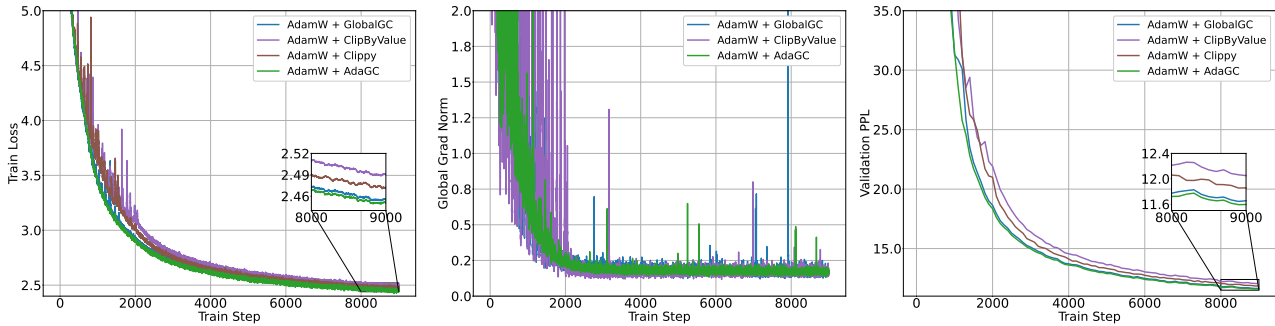


Figure 7. Llama-2 1.3B training dynamics of clipping methods.

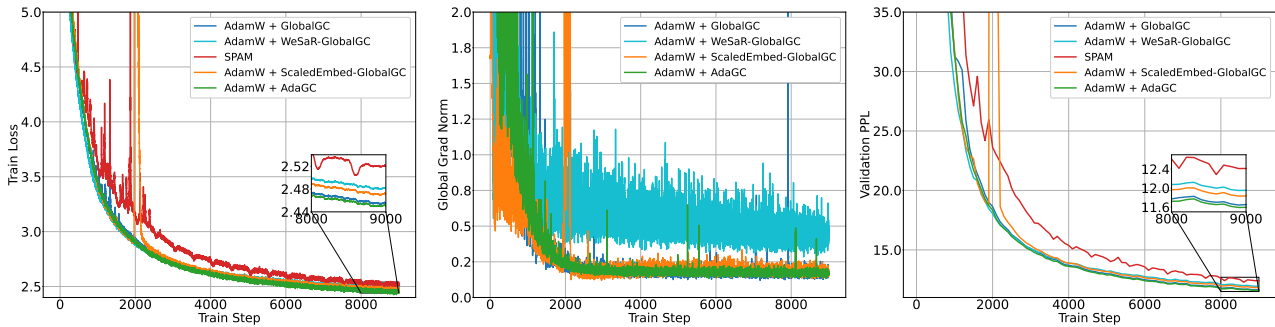


Figure 8. Llama-2 1.3B training dynamics of other baseline methods.

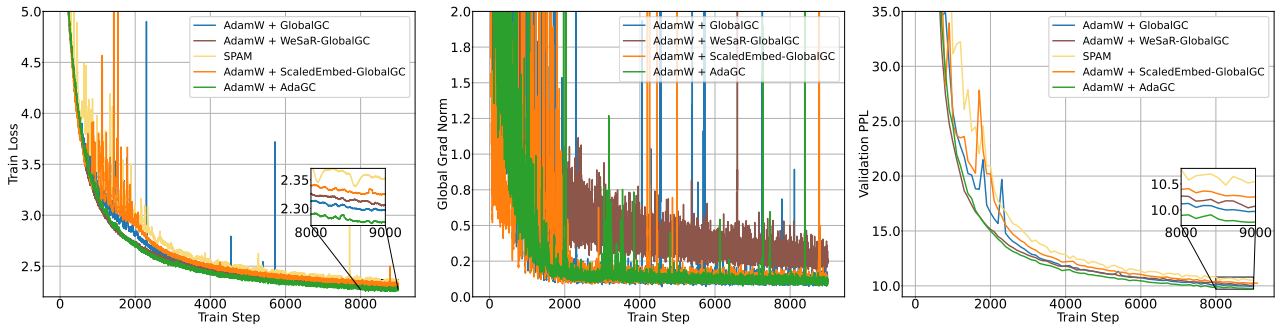


Figure 9. Llama-2 7B training dynamics of other baseline methods.

E.2. Optimizer State Dynamics

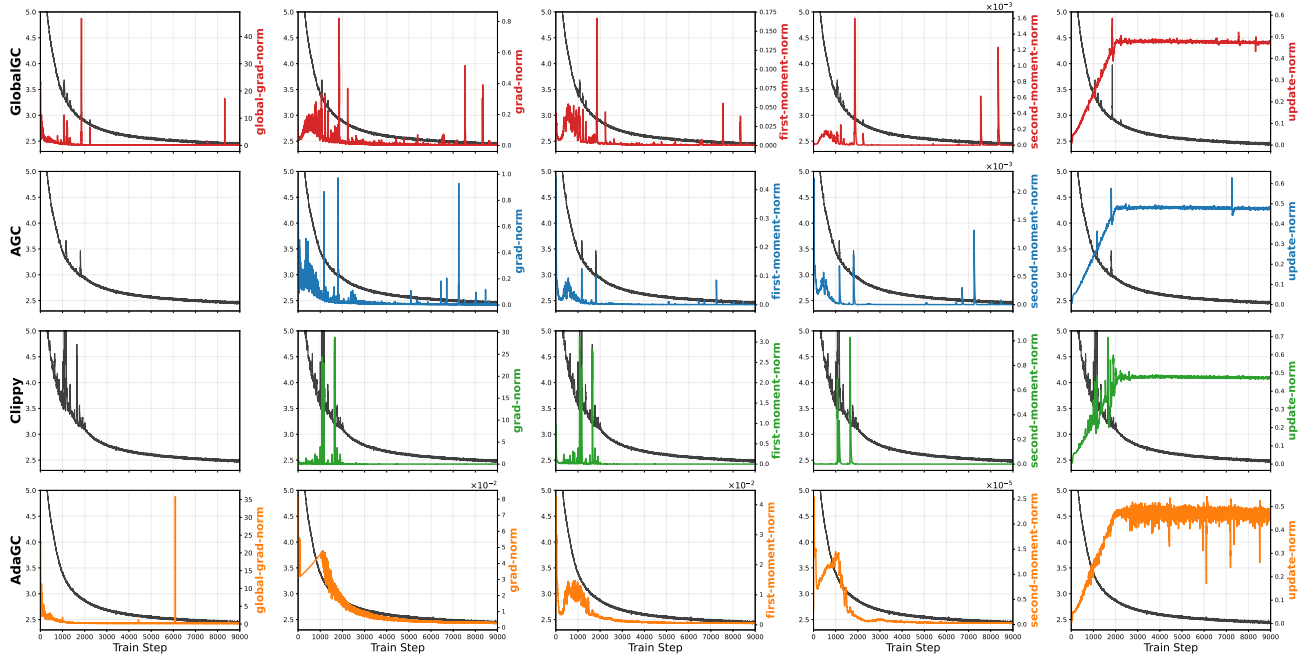


Figure 10. Visualization of the gradient norm, first-moment norm, second-moment norm, update norm, loss, and global gradient norm for the embedding of Llama-2 1.3B. Each row represents a different clipping method: the first row is GlobalGC, the second is AGC, the third is Clippy, and the fourth is our AdaGC. The black curve in each plot shows the loss trajectory.

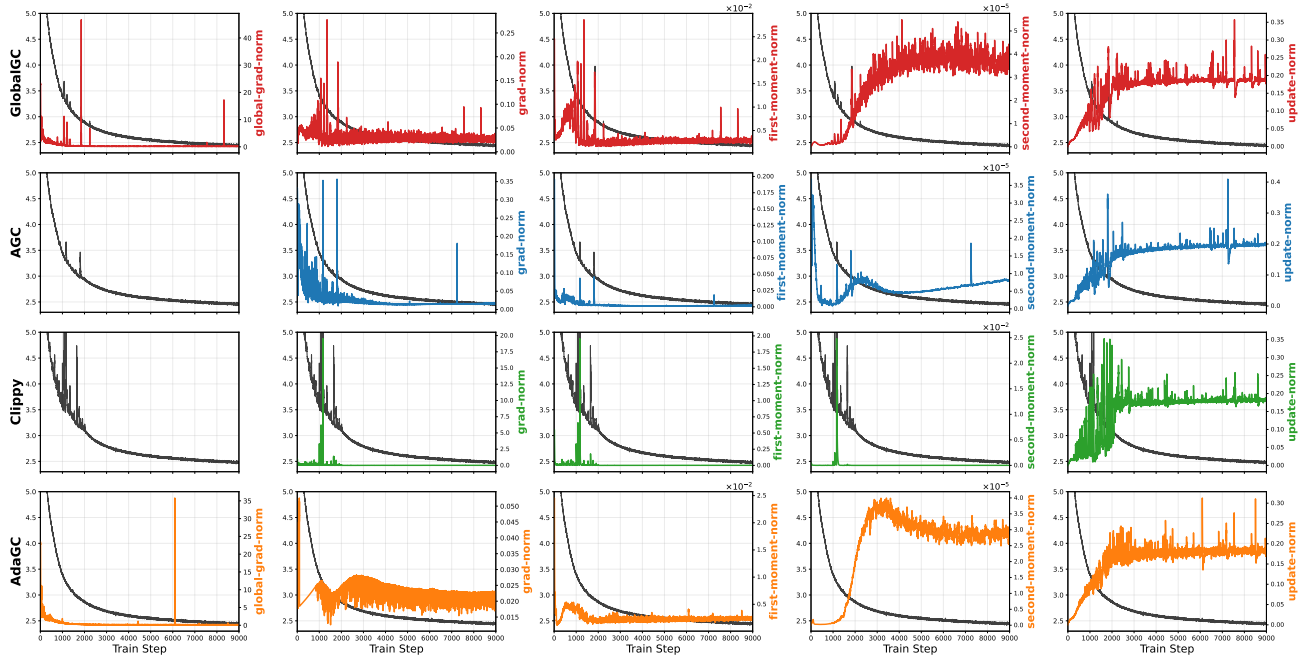


Figure 11. Visualization of the gradient norm, first-moment norm, second-moment norm, update norm, loss, and global gradient norm for the encoder_layers_3_self_attention_query_key_value of Llama-2 1.3B. Each row represents a different clipping method: the first row is GlobalGC, the second is AGC, the third is Clippy, and the fourth is our AdaGC. The black curve in each plot shows the loss trajectory.

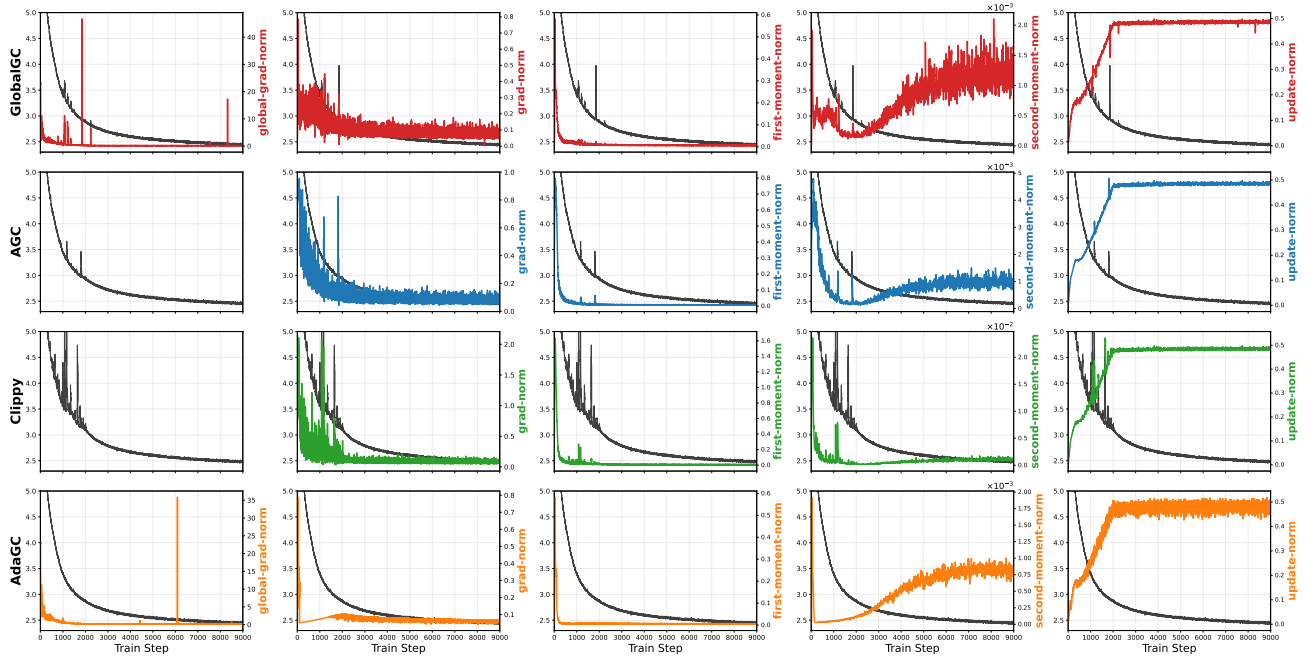


Figure 12. Visualization of the gradient norm, first-moment norm, second-moment norm, update norm, loss, and global gradient norm for the LMHead of Llama-2 1.3B. Each row represents a different clipping method: the first row is GlobalGC, the second is AGC, the third is Clippy, and the fourth is our AdaGC. The black curve in each plot shows the loss trajectory.

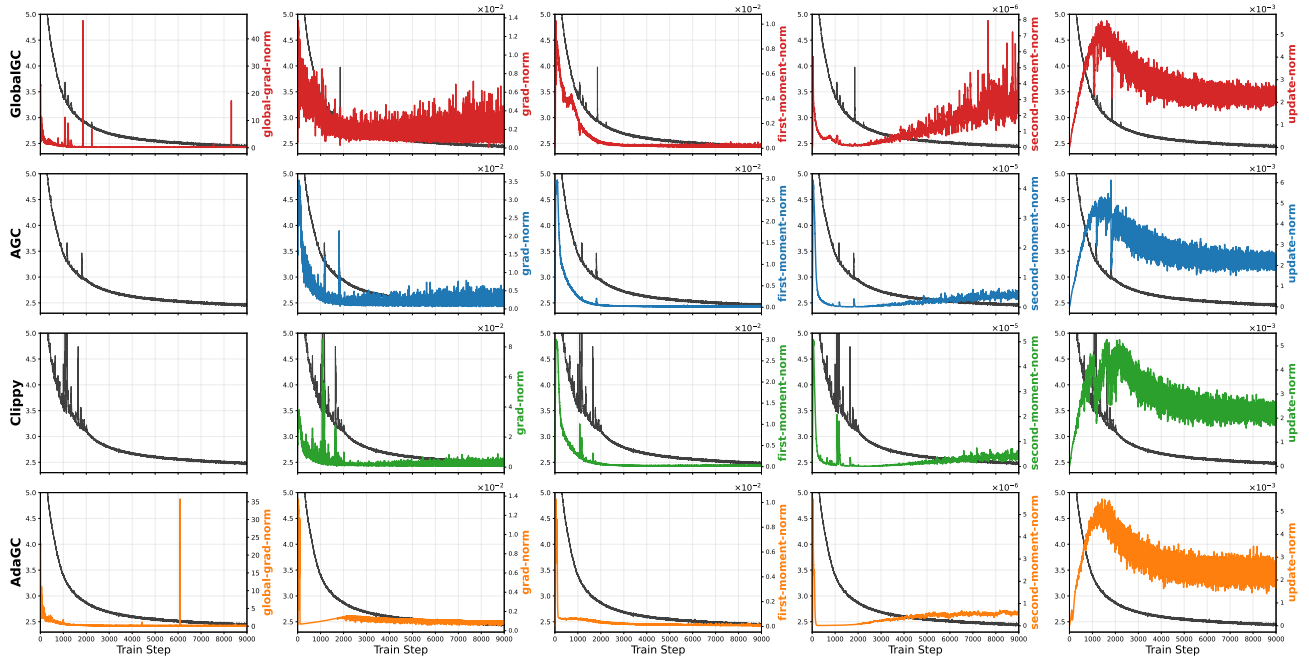


Figure 13. Visualization of the gradient norm, first-moment norm, second-moment norm, update norm, loss, and global gradient norm for the encoder_final_layernorm of Llama-2 1.3B. Each row represents a different clipping method: the first row is GlobalGC, the second is AGC, the third is Clippy, and the fourth is our AdaGC. The black curve in each plot shows the loss trajectory.

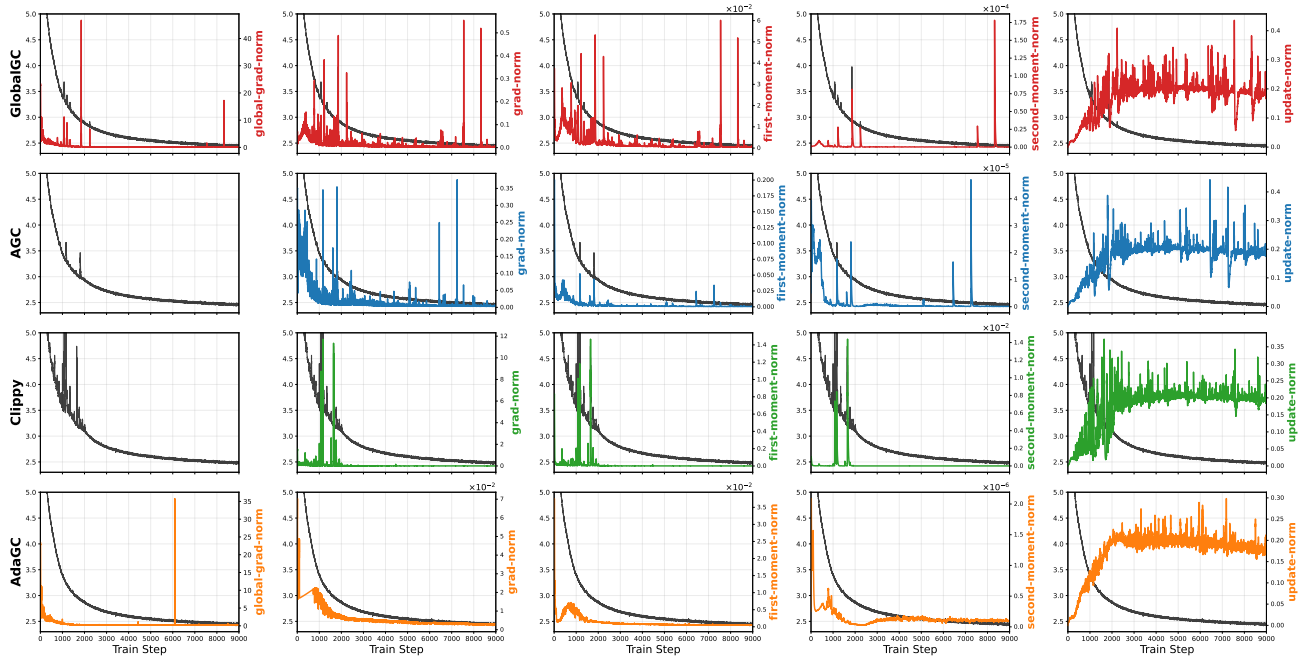


Figure 14. Visualization of the gradient norm, first-moment norm, second-moment norm, update norm, loss, and global gradient norm for the `encoder_layers_0_self_attention_query_key_value` of Llama-2 1.3B. Each row represents a different clipping method: the first row is GlobalGC, the second is AGC, the third is Clippy, and the fourth is our AdaGC. The black curve in each plot shows the loss trajectory.

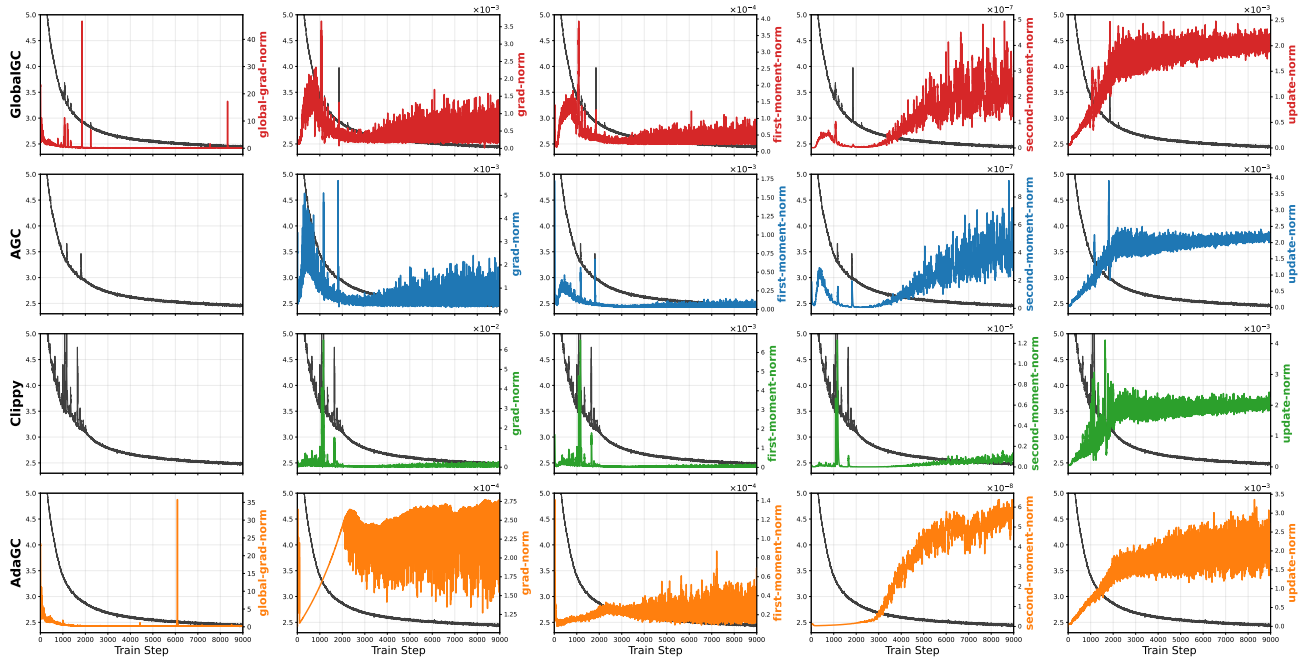


Figure 15. Visualization of the gradient norm, first-moment norm, second-moment norm, update norm, loss, and global gradient norm for the `encoder_layers_23_input_layernorm` of Llama-2 1.3B. Each row represents a different clipping method: the first row is GlobalGC, the second is AGC, the third is Clippy, and the fourth is our AdaGC. The black curve in each plot shows the loss trajectory.

F. Convergence Analysis and Proof

Any operation that modifies gradients may potentially result in non-convergence. In this section, rather than providing a theoretical guarantee that AdaGC eliminates loss spikes, we present the convergence guarantee for Adam with AdaGC, stated as follows:

Theorem F.1. *Under mild assumptions, by selecting $\alpha_t = \mathcal{O}(1/\sqrt{T})$, $\beta_2 = 1 - \mathcal{O}(1/T)$ and $\beta_1 < \sqrt{\beta_2}$, when τ is randomly chosen from $\{1, 2, \dots, T\}$ with equal probabilities, it holds that*

$$\mathbb{E}\|\nabla f(\theta_\tau)\|^2 = \mathcal{O}\left(\frac{1}{\sqrt{T}}\right).$$

Theorem F.1 shows that even with local clipped gradient, Adam with AdaGC can converge at the same rate as vanilla Adam (Kingma & Ba, 2014).

In the following, we provide the necessary assumptions and lemmas for the proofs of Theorem F.1.

Notations The k -th component of a vector v_t is denoted as $v_{t,k}$. Other than that, all computations that involve vectors shall be understood in the component-wise way. We say a vector $v_t \geq 0$ if every component of v_t is non-negative, and $v_t \geq w_t$ if $v_{t,k} \geq w_{t,k}$ for all $k = 1, 2, \dots, d$. The ℓ_1 norm of a vector v_t is defined as $\|v_t\|_1 = \sum_{k=1}^d |v_{t,k}|$. The ℓ_2 norm is defined as $\|v_t\|^2 = \langle v_t, v_t \rangle = \sum_{k=1}^d |v_{t,k}|^2$. Given a positive vector $\hat{\eta}_t$, it will be helpful to define the following weighted norm: $\|v_t\|_{\hat{\eta}_t}^2 = \langle v_t, \hat{\eta}_t v_t \rangle = \sum_{k=1}^d \hat{\eta}_{t,k} |v_{t,k}|^2$.

Assumption F.2. The function f is lower bounded by \underline{f} with L -Lipschitz gradient.

Assumption F.3. The gradient estimator g is unbiased with bounded norm, e.g.,

$$\mathbb{E}[g|x_t] = \nabla f(x_t), \quad \|g_t\| \leq G.$$

Assumption F.4. The coefficient of clipping $h_{t,i}$ is lower bounded by some $h_0 > 0$.

Assumption F.5. $\|g_t - \nabla f(x_t)\| \leq p \|\nabla f(x_t)\|$ holds for some $p < 1$ and for all t .

Remark F.6. Assumption F.2 and Assumption F.3 are widely used in the proof of optimization algorithm with adaptive learning rates (Reddi et al., 2018). Assumption F.4 is because the gradient norm changes slowly when training the neural network, and the last assumption holds when the batch size is large enough.

Lemma F.7. *Let $\zeta := \beta_1^2/\beta_2$. We have the following estimate*

$$m_t^2 \leq \frac{1}{(1-\zeta)(1-\beta_2)} v_t, \quad \forall t. \quad (4)$$

Proof. By the iteration formula $m_t = \beta_1 m_{t-1} + (1-\beta_1)\hat{g}_t$ and $m_0 = 0$, we have

$$m = \sum_{i=1}^t \beta_1^{t-i} (1-\beta_1)\hat{g}_i.$$

Similarly, by $v_t = \beta_2 v_{t-1} + (1-\beta_2)\hat{g}_t^2$ and $v_0 = 0$, we have

$$v_t = \sum_{i=1}^t \beta_2^{t-i} (1-\beta_2)\hat{g}_i^2$$

It follows by arithmetic inequality that

$$\begin{aligned} m_t^2 &= \left(\sum_{i=1}^t \frac{(1-\beta_1)\beta_1^{t-i}}{\sqrt{(1-\beta_2)\beta_2^{t-i}}} \sqrt{(1-\beta_2)\beta_2^{t-i}} \hat{g}_i \right)^2 \\ &\leq \left(\sum_{i=1}^t \frac{(1-\beta_1)^2 \beta_1^{2(t-i)}}{(1-\beta_2)\beta_2^{t-i}} \right) \left(\sum_{i=1}^t (1-\beta_2)\beta_2^{t-i} \hat{g}_i^2 \right) = \left(\sum_{i=1}^t \frac{(1-\beta_1)^2 \beta_1^{2(t-i)}}{(1-\beta_2)\beta_2^{t-i}} \right) v_t. \end{aligned}$$

Further, we have

$$\sum_{i=1}^t \frac{(1-\beta_1)^2 \beta_1^{2(t-i)}}{(1-\beta_2)\beta_2^{t-i}} \leq \frac{1}{1-\beta_2} \sum_{i=1}^t \left(\frac{\beta_1^2}{\beta_2}\right)^{t-i} = \frac{1}{1-\beta_2} \sum_{k=0}^{t-1} \zeta^k \leq \frac{1}{(1-\zeta)(1-\beta_2)}.$$

The proof is completed. \square

Lemma F.8. *The following estimate holds*

$$\sum_{t=1}^T \|\Delta_t\|^2 \leq \frac{\alpha^2 G^2}{\epsilon}$$

Proof. By using the definition of m_t , it holds $\|m_t\|^2 \leq G^2$.

Then, $\|\Delta_t\|^2 = \left\| \frac{\alpha_t m_t}{\sqrt{\hat{v}_t + \epsilon}} \right\|^2 \leq \frac{G^2}{\epsilon} \alpha_t^2$ by using the definition of Δ_t .

Therefore, $\sum_{t=1}^T \|\Delta_t\|^2 \leq \frac{G^2}{\epsilon} \sum_{t=1}^T \frac{\alpha_t^2}{T} = \frac{G^2 \alpha^2}{\epsilon}$. \square

Lemma F.9. *With the Assumption F.4 and F.5, it holds that*

$$\mathbb{E} \langle \nabla f(\theta_t), \hat{\eta}_t \hat{g}_t \rangle \geq h_0 \mathbb{E} \|\nabla f(\theta_t)\|_{\hat{\eta}_t}^2.$$

Proof. According to Assumption F.5, it holds that

$$\begin{aligned} \langle \nabla_i f(\theta_t), g_{t,i} \rangle &= -\frac{1}{2} \left(\|\nabla_i f(\theta_t) - g_{t,i}\|^2 - \|\nabla_i f(\theta_t)\|^2 - \|g_{t,i}\|^2 \right) \\ &\geq (1-p^2) \|\nabla_i f(\theta_t)\|^2 \geq 0. \end{aligned}$$

Thus, it holds that

$$\begin{aligned} \mathbb{E} [\langle \nabla f(x_t), \hat{\eta}_t \hat{g}_t \rangle] &= \mathbb{E} \left[\sum_i \langle \nabla_i f(\theta_t), h_{t,i} \hat{\eta}_{t,i} g_{t,i} \rangle \right] \\ &\geq h_0 \mathbb{E} \left[\sum_i \langle \nabla_i f(x_t), h_{t,i} \hat{\eta}_{t,i} g_{t,i} \rangle \right] \\ &= h_0 \mathbb{E} \langle \nabla f(\theta_t), \hat{\eta}_t g_t \rangle = h_0 \mathbb{E} \|\nabla f(\theta_t)\|_{\hat{\eta}_t}^2. \end{aligned}$$

\square

Let $\Delta_t := \theta_{t+1} - \theta_t = -\alpha_t m_t / (\sqrt{\hat{v}_t} + \epsilon)$. Let $\hat{v}_t = \beta_2 v_{t-1} + (1-\beta_2)\delta_t^2$, where $\delta_t^2 = \mathbb{E}_t [\hat{g}_t^2]$ and let $\hat{\eta}_t = \alpha_t / \sqrt{\hat{v}_t + \epsilon}$.

Lemma F.10. *Let $M_t = \mathbb{E} [\langle \nabla f(\theta_t), \Delta_t \rangle + L \|\Delta_t\|^2]$. Let $\alpha_t = \alpha / \sqrt{T}$ and $\beta_2 = 1 - \beta/T$. Then, for $T \geq 1$ we have*

$$\sum_{t=1}^T M_t \leq \frac{C_2}{1-\sqrt{\zeta}} + \frac{LG^2\alpha^2}{(1-\sqrt{\zeta})\epsilon} - \frac{(1-\beta_1)h_0}{2} \sum_{t=1}^T \mathbb{E} \|\nabla f(\theta_t)\|_{\hat{\eta}_t}^2, \quad (5)$$

where $C_2 = \frac{5}{2(1-\beta_1)h_0} \left((1-\beta_1)^2 \frac{4\alpha\beta G^4}{\epsilon^3} + \beta_1^2 \alpha \beta \left(\frac{G^4}{\beta_2 \epsilon^3} + \frac{(1+\epsilon)G^2}{(1-\zeta)\epsilon\beta_2} + \frac{G^4}{\beta_2} \right) \right)$.

Proof. To split M_t , firstly we introduce the following two equalities. Using the definitions of v_t and \hat{v}_t , we obtain

$$\begin{aligned} \frac{(1-\beta_1)\alpha_t\hat{g}_t}{\sqrt{v_t}+\epsilon} &= \frac{(1-\beta_1)\alpha_t\hat{g}_t}{\sqrt{\hat{v}_t}+\epsilon} + (1-\beta_1)\alpha_t\hat{g}_t\left(\frac{1}{\sqrt{v_t}+\epsilon} - \frac{1}{\sqrt{\hat{v}_t}+\epsilon}\right) \\ &= (1-\beta_1)\hat{\eta}_t\hat{g}_t + (1-\beta_1)\alpha_t\hat{g}_t\frac{(1-\beta_2)(\sigma_t^2-\hat{g}_t^2)}{(\sqrt{v_t}+\epsilon)(\sqrt{\hat{v}_t}+\epsilon)(\sqrt{v_t}+\sqrt{\hat{v}_t})} \\ &= (1-\beta_1)\hat{\eta}_t\hat{g}_t + (1-\beta_1)\hat{\eta}_t\hat{g}_t\frac{(1-\beta_2)(\sigma_t^2-\hat{g}_t^2)}{(\sqrt{v_t}+\epsilon)(\sqrt{v_t}+\sqrt{\hat{v}_t})} \end{aligned}$$

In addition, we can obtain:

$$\begin{aligned} &\beta_1\alpha_tm_{t-1}\left(\frac{1}{\sqrt{\beta_2v_{t-1}}+\sqrt{\beta_2\epsilon}} - \frac{1}{\sqrt{v_t}+\epsilon}\right) \\ &= \beta_1\alpha_tm_{t-1}\frac{(1-\beta_2)\hat{g}_t^2}{(\sqrt{v_t}+\epsilon)(\sqrt{\beta_2v_{t-1}}+\sqrt{\beta_2\epsilon})(\sqrt{v_t}+\sqrt{\beta_2v_{t-1}})} + \beta_1\alpha_tm_{t-1}\frac{(1-\sqrt{\beta_2})\epsilon}{(\sqrt{v_t}+\epsilon)(\sqrt{\beta_2v_{t-1}}+\sqrt{\beta_2\epsilon})} \\ &= \beta_1\alpha_tm_{t-1}\frac{(1-\beta_2)\hat{g}_t^2}{(\sqrt{\hat{v}_t}+\epsilon)(\sqrt{\beta_2v_{t-1}}+\sqrt{\beta_2\epsilon})(\sqrt{v_t}+\sqrt{\beta_2v_{t-1}})} \\ &\quad + \beta_1\alpha_tm_{t-1}\frac{(1-\beta_2)\hat{g}_t^2}{(\sqrt{\beta_2v_{t-1}}+\sqrt{\beta_2\epsilon})(\sqrt{v_t}+\sqrt{\beta_2v_{t-1}})}\left(\frac{1}{\sqrt{\hat{v}_t}+\epsilon} - \frac{1}{\sqrt{v_t}+\epsilon}\right) \\ &\quad + \beta_1\alpha_tm_{t-1}\frac{(1-\sqrt{\beta_2})\epsilon}{(\sqrt{v_t}+\epsilon)(\sqrt{\beta_2v_{t-1}}+\sqrt{\beta_2\epsilon})} + \beta_1\alpha_tm_{t-1}\frac{(1-\sqrt{\beta_2})\epsilon}{\sqrt{\beta_2v_{t-1}}+\sqrt{\beta_2\epsilon}}\left(\frac{1}{\sqrt{\hat{v}_t}+\epsilon} - \frac{1}{\sqrt{v_t}+\epsilon}\right) \\ &= \beta_1m_{t-1}\hat{\eta}_t\frac{(1-\beta_2)\hat{g}_t^2}{(\sqrt{\beta_2v_{t-1}}+\sqrt{\beta_2\epsilon})(\sqrt{v_t}+\sqrt{\beta_2v_{t-1}})} \\ &\quad + \beta_1\hat{\eta}_tm_{t-1}\frac{(1-\beta_2)^2\hat{g}_t^2(\sigma_t^2-\hat{g}_t^2)}{(\sqrt{v_t}+\epsilon)(\sqrt{v_t}+\sqrt{\hat{v}_t})(\sqrt{\beta_2v_{t-1}}+\sqrt{\beta_2\epsilon})(\sqrt{v_t}+\sqrt{\beta_2v_{t-1}})} \\ &\quad + \beta_1\hat{\eta}_tm_{t-1}\frac{(1-\sqrt{\beta_2})\epsilon}{\sqrt{\beta_2v_{t-1}}+\sqrt{\beta_2\epsilon}} + \beta_1\hat{\eta}_tm_{t-1}\frac{(1-\sqrt{\beta_2})(1-\beta_2)\epsilon(\sigma_t^2-\hat{g}_t^2)}{(\sqrt{v_t}+\epsilon)(\sqrt{v_t}+\sqrt{\hat{v}_t})(\sqrt{\beta_2v_{t-1}}+\sqrt{\beta_2\epsilon})}. \end{aligned}$$

For simplicity, we denote

$$\begin{aligned} A_t^1 &= (1-\beta_1)\sqrt{\hat{\eta}_t}\hat{g}_t\frac{(1-\beta_2)(\sigma_t^2-\hat{g}_t^2)}{(\sqrt{v_t}+\epsilon)(\sqrt{v_t}+\sqrt{\hat{v}_t})} \\ A_t^2 &= \beta_1m_{t-1}\sqrt{\hat{\eta}_t}\frac{(1-\beta_2)\hat{g}_t^2}{(\sqrt{\beta_2v_{t-1}}+\sqrt{\beta_2\epsilon})(\sqrt{v_t}+\sqrt{\beta_2v_{t-1}})} \\ A_t^3 &= \beta_1\sqrt{\hat{\eta}_t}m_{t-1}\frac{(1-\beta_2)^2\hat{g}_t^2(\sigma_t^2-\hat{g}_t^2)}{(\sqrt{v_t}+\epsilon)(\sqrt{v_t}+\sqrt{\hat{v}_t})(\sqrt{\beta_2v_{t-1}}+\sqrt{\beta_2\epsilon})(\sqrt{v_t}+\sqrt{\beta_2v_{t-1}})} \\ A_t^4 &= \beta_1\sqrt{\hat{\eta}_t}m_{t-1}\frac{(1-\sqrt{\beta_2})\epsilon}{\sqrt{\beta_2v_{t-1}}+\sqrt{\beta_2\epsilon}} \\ A_t^5 &= \beta_1\sqrt{\hat{\eta}_t}m_{t-1}\frac{(1-\sqrt{\beta_2})(1-\beta_2)\epsilon(\sigma_t^2-\hat{g}_t^2)}{(\sqrt{v_t}+\epsilon)(\sqrt{v_t}+\sqrt{\hat{v}_t})(\sqrt{\beta_2v_{t-1}}+\sqrt{\beta_2\epsilon})} \end{aligned}$$

Then, we obtain

$$\begin{aligned} \Delta_t - \frac{\beta_1\alpha_t}{\sqrt{\beta_2\alpha_{t-1}}}\Delta_{t-1} &= -\frac{\alpha_tm_t}{\sqrt{v_t}+\epsilon} + \frac{\beta_1\alpha_tm_{t-1}}{\sqrt{\beta_2v_{t-1}}+\sqrt{\beta_2\epsilon}} \\ &= -\frac{(1-\beta_1)\alpha_t\hat{g}_t}{\sqrt{v_t}+\epsilon} + \beta_1\alpha_tm_{t-1}\left(\frac{1}{\sqrt{\beta_2v_{t-1}}+\sqrt{\beta_2\epsilon}} - \frac{1}{\sqrt{v_t}+\epsilon}\right) \\ &= -(1-\beta_1)\hat{\eta}_t\hat{g}_t - \sqrt{\hat{\eta}_t}A_t^1 + \sqrt{\hat{\eta}_t}A_t^2 + \sqrt{\hat{\eta}_t}A_t^3 + \sqrt{\hat{\eta}_t}A_t^4 + \sqrt{\hat{\eta}_t}A_t^5 \end{aligned}$$

Thus, it holds that

$$\begin{aligned}
 \mathbb{E} \langle \nabla f(\theta_t), \Delta_t \rangle &= \frac{\beta_1 \alpha_t}{\sqrt{\beta_2 \alpha_{t-1}}} \langle \nabla f(\theta_t), \Delta_{t-1} \rangle + \mathbb{E} \left\langle \nabla f(\theta_t), \Delta_t - \frac{\beta_1 \alpha_t}{\sqrt{\beta_2 \alpha_{t-1}}} \Delta_{t-1} \right\rangle \\
 &= \frac{\beta_1 \alpha_t}{\sqrt{\beta_2 \alpha_{t-1}}} (\mathbb{E} \langle \nabla f(\theta_t), \Delta_{t-1} \rangle + \mathbb{E} \langle \nabla f(\theta_t) - \nabla f(\theta_{t-1}), \Delta_{t-1} \rangle) \\
 &\quad + \mathbb{E} \langle \nabla f(\theta_t), -(1 - \beta_1) \hat{\eta}_t \hat{g}_t \rangle + \mathbb{E} \langle \nabla f(\theta_t), -\sqrt{\hat{\eta}_t} A_t^1 \rangle + \mathbb{E} \langle \nabla f(\theta_t), \sqrt{\hat{\eta}_t} A_t^2 \rangle \\
 &\quad + \mathbb{E} \langle \nabla f(\theta_t), \sqrt{\hat{\eta}_t} A_t^3 \rangle + \mathbb{E} \langle \nabla f(\theta_t), \sqrt{\hat{\eta}_t} A_t^4 \rangle + \mathbb{E} \langle \nabla f(\theta_t), \sqrt{\hat{\eta}_t} A_t^5 \rangle
 \end{aligned} \tag{6}$$

For the first term of (6), it holds that

$$\begin{aligned}
 &\frac{\beta_1 \alpha_t}{\sqrt{\beta_2 \alpha_{t-1}}} (\mathbb{E} \langle \nabla f(\theta_t), \Delta_{t-1} \rangle + \mathbb{E} \langle \nabla f(\theta_t) - \nabla f(\theta_{t-1}), \Delta_{t-1} \rangle) \\
 &\leq \frac{\beta_1 \alpha_t}{\sqrt{\beta_2 \alpha_{t-1}}} (\mathbb{E} \langle \nabla f(\theta_t), \Delta_{t-1} \rangle + \mathbb{E} \|\nabla f(\theta_t) - \nabla f(\theta_{t-1})\| \|\Delta_{t-1}\|) \\
 &\leq \frac{\beta_1 \alpha_t}{\sqrt{\beta_2 \alpha_{t-1}}} (\mathbb{E} \langle \nabla f(\theta_t), \Delta_{t-1} \rangle + L \mathbb{E} \|\Delta_{t-1}\|^2) \\
 &= \frac{\beta_1 \alpha_t}{\sqrt{\beta_2 \alpha_{t-1}}} M_{t-1}
 \end{aligned}$$

For the second term of (6), it holds that

$$\mathbb{E} \langle \nabla f(\theta_t), -(1 - \beta_1) \hat{\eta}_t \hat{g}_t \rangle \leq -(1 - \beta_1) h_0 \mathbb{E} \|\nabla f(\theta_t)\|_{\hat{\eta}_t}^2.$$

For the rest of the terms, it holds that

$$\begin{aligned}
 \mathbb{E} \langle \nabla f(\theta_t), -\sqrt{\hat{\eta}_t} A_t^1 \rangle &\leq \frac{h_0(1 - \beta_1)}{10} \mathbb{E} \|\nabla f(\theta_t)\|_{\hat{\eta}_t}^2 + \frac{5}{2(1 - \beta_1)h_0} \|A_t^1\|^2 \\
 \mathbb{E} \langle \nabla f(\theta_t), +\sqrt{\hat{\eta}_t} A_t^2 \rangle &\leq \frac{h_0(1 - \beta_1)}{10} \mathbb{E} \|\nabla f(\theta_t)\|_{\hat{\eta}_t}^2 + \frac{5}{2(1 - \beta_1)h_0} \|A_t^2\|^2 \\
 \mathbb{E} \langle \nabla f(\theta_t), +\sqrt{\hat{\eta}_t} A_t^3 \rangle &\leq \frac{h_0(1 - \beta_1)}{10} \mathbb{E} \|\nabla f(\theta_t)\|_{\hat{\eta}_t}^2 + \frac{5}{2(1 - \beta_1)h_0} \|A_t^3\|^2 \\
 \mathbb{E} \langle \nabla f(\theta_t), +\sqrt{\hat{\eta}_t} A_t^4 \rangle &\leq \frac{h_0(1 - \beta_1)}{10} \mathbb{E} \|\nabla f(\theta_t)\|_{\hat{\eta}_t}^2 + \frac{5}{2(1 - \beta_1)h_0} \|A_t^4\|^2 \\
 \mathbb{E} \langle \nabla f(\theta_t), +\sqrt{\hat{\eta}_t} A_t^5 \rangle &\leq \frac{h_0(1 - \beta_1)}{10} \mathbb{E} \|\nabla f(\theta_t)\|_{\hat{\eta}_t}^2 + \frac{5}{2(1 - \beta_1)h_0} \|A_t^5\|^2
 \end{aligned}$$

On the other hand, it holds that

$$\begin{aligned}
 \|A_t^1\|^2 &\leq (1 - \beta_1)^2 \frac{4\alpha\beta G^4}{T\epsilon^3}, \|A_t^2\|^2 \leq \beta_1^2 \frac{\alpha\beta G^4}{T\beta_2\epsilon^3}, \|A_t^3\|^2 \leq \beta_1^2 \frac{\alpha\beta G^2}{(1 - \zeta)\epsilon T\beta_2}, \\
 \|A_t^4\|^2 &\leq \beta_1^2 \frac{\alpha\beta G^4}{T\beta_2}, \|A_t^5\|^2 \leq \beta_1^2 \frac{\alpha\beta G^2}{(1 - \zeta)\beta_2 T}
 \end{aligned}$$

□

Define $N_t = \frac{C_2}{T} + L \mathbb{E} \|\Delta_t\|^2$, where $C_2 = \frac{5}{2(1 - \beta_1)h_0} \left((1 - \beta_1)^2 \frac{4\alpha\beta G^4}{\epsilon^3} + \beta_1^2 \alpha\beta \left(\frac{G^4}{\beta_2\epsilon^3} + \frac{(1 + \epsilon)G^2}{(1 - \zeta)\epsilon\beta_2} + \frac{G^4}{\beta_2} \right) \right)$. It holds that

$$M_t \leq \frac{\beta_1 \alpha_t}{\sqrt{\beta_2 \alpha_{t-1}}} M_{t-1} + N_t - \frac{1 - \beta_1}{2} \hat{\eta}_t \mathbb{E} \|\nabla f(\theta_t)\|_{\hat{\eta}_t}^2 \leq \sum_{i=1}^t \sqrt{\zeta}^{t-i} N_i - \frac{1 - \beta_1}{2} h_0 \mathbb{E} \|\nabla f(\theta_t)\|_{\hat{\eta}_t}^2$$

Thus, by summing t from 1 to T , it holds that

$$\begin{aligned} \sum_{t=1}^T M_t &\leq \sum_{t=1}^T \sum_{i=1}^t \sqrt{\zeta}^{t-i} N_i - \frac{(1-\beta_1)h_0}{2} \mathbb{E} \|\nabla f(\theta_t)\|_{\hat{\eta}_t}^2 \\ &\leq \frac{1}{1-\sqrt{\zeta}} \sum_{t=1}^T N_t - \frac{(1-\beta_1)h_0}{2} \mathbb{E} \|\nabla f(\theta_t)\|_{\hat{\eta}_t}^2 \\ &\leq \frac{C_2}{1-\sqrt{\zeta}} + \frac{LG^2\alpha^2}{(1-\sqrt{\zeta})\epsilon} - \frac{(1-\beta_1)h_0}{2} \sum_{t=1}^T \mathbb{E} \|\nabla f(\theta_t)\|_{\hat{\eta}_t}^2. \end{aligned}$$

Lemma F.11. *Let τ be randomly chosen from $\{1, 2, \dots, T\}$ with equal probabilities $p_\tau = \frac{1}{T}$. We have the following estimate:*

$$\mathbb{E} [\|\nabla f(\theta_\tau)\|^2] \leq \frac{\sqrt{G^2 + \epsilon d}}{\alpha\sqrt{T}} \mathbb{E} \left[\sum_{t=1}^T \|\nabla f(\theta_t)\|_{\hat{\eta}_t}^2 \right].$$

Proof. Note that $\|\hat{v}_t\|_1 = \beta_2 \|v_{t-1}\|_1 + (1-\beta_2) \|\sigma_t\|^2$ and $\|\hat{g}_t\| \leq G$. It is straightforward to prove $\|v_t\|_1 \leq G^2$. Hence, we have $\|\hat{v}_t + \epsilon\|_1 \leq G^2 + \epsilon d$.

Utilizing this inequality, we have

$$\begin{aligned} \|\nabla f(\theta_t)\|^2 &= \frac{\|\nabla f(\theta_t)\|^2}{\sqrt{\|\hat{v}_t + \epsilon\|_1}} \sqrt{\|\hat{v}_t + \epsilon\|_1} = \sqrt{\|\hat{v}_t + \epsilon\|_1} \sum_{k=1}^d \frac{|\nabla_k f(\theta_t)|^2}{\sqrt{\sum_{l=1}^d \hat{v}_{t,l} + \epsilon}} \\ &\leq \sqrt{\|\hat{v}_t + \epsilon\|_1} \alpha_t^{-1} \sum_{k=1}^d \frac{\alpha_t}{\sqrt{\hat{v}_{t,k} + \epsilon}} |\nabla_k f(\theta_t)|^2 = \sqrt{\|\hat{v}_t + \epsilon\|_1} \alpha_t^{-1} \|\nabla f(\theta_t)\|_{\hat{\eta}_t}^2 \\ &\leq \sqrt{G^2 + \epsilon d} \alpha_t^{-1} \|\nabla f(\theta_t)\|_{\hat{\eta}_t}^2 \leq \frac{\sqrt{G^2 + \epsilon d}}{\alpha_T} \|\nabla f(\theta_t)\|_{\hat{\eta}_t}^2. \end{aligned}$$

Then, by using the definition of θ_τ , we obtain

$$\mathbb{E} [\|\nabla f(\theta_\tau)\|^2] = \frac{1}{T} \sum_{t=1}^T \mathbb{E} [\|\nabla f(\theta_t)\|^2] \leq \frac{\sqrt{G^2 + \epsilon d}}{\alpha\sqrt{T}} \mathbb{E} \left[\sum_{t=1}^T \|\nabla f(\theta_t)\|_{\hat{\eta}_t}^2 \right].$$

Thus, the desired result is obtained. \square

Theorem F.12. *Let $\{\theta_t\}$ be a sequence generated by AdaGC for initial values θ_1 and $m_0 = v_0 = 0$. Assumptions F.2 to F.5 hold. With the hyperparameters $\alpha_t = \alpha/\sqrt{T}$, $\beta_2 = 1 - \beta/T$ and $\zeta = \beta_1^2/\beta_2 < 1$. Let τ be randomly chosen from $\{1, 2, \dots, T\}$ with equal probabilities. We have*

$$\mathbb{E} \|\nabla f(\theta_\tau)\|^2 \leq \frac{C}{\sqrt{T}}$$

where $C = \frac{\sqrt{G^2 + \epsilon d}}{\alpha} \left(f(\theta_1) - \underline{f} + \frac{C_2}{1-\sqrt{\zeta}} + \frac{LG^2\alpha^2}{(1-\sqrt{\zeta})\epsilon} \right)$ and $C_2 = \frac{5}{2(1-\beta_1)h_0} \left((1-\beta_1)^2 \frac{4\alpha\beta G^4}{\epsilon^3} + \beta_1^2 \alpha \beta \left(\frac{G^4}{\beta_2 \epsilon^3} + \frac{(1+\epsilon)G^2}{(1-\zeta)\epsilon\beta_2} + \frac{G^4}{\beta_2} \right) \right)$.

Proof. With the Lipschitz continuity condition of f , it holds that

$$\mathbb{E} f(\theta_{t+1}) \leq \mathbb{E} \left[f(\theta_t) + \langle \nabla f(\theta_t), \Delta_t \rangle + \frac{L}{2} \|\Delta_t\|^2 \right] \leq \mathbb{E} f(\theta_t) + M_t.$$

By summing t from 1 to T , it holds that

$$\mathbb{E} f(\theta_{T+1}) \leq f(\theta_1) + \sum_{t=1}^T M_t \leq f(\theta_1) + \frac{C_2}{1-\sqrt{\zeta}} + \frac{LG^2\alpha^2}{(1-\sqrt{\zeta})\epsilon} - \frac{(1-\beta_1)h_0}{2} \sum_{t=1}^T \mathbb{E} \|\nabla f(\theta_t)\|_{\hat{\eta}_t}^2$$

Thus, it holds that

$$\begin{aligned}
 \mathbb{E} [\|\nabla f(\theta_\tau)\|^2] &\leq \frac{\sqrt{G^2 + \epsilon d}}{\alpha\sqrt{T}} \mathbb{E} \left[\sum_{t=1}^T \|\nabla f(\theta_t)\|_{\tilde{\eta}_t}^2 \right] \\
 &\leq \frac{\sqrt{G^2 + \epsilon d}}{\alpha\sqrt{T}} \left(f(\theta_1) - \mathbb{E}[f(\theta_{T+1})] + \frac{C_2}{1 - \sqrt{\zeta}} + \frac{LG^2\alpha^2}{(1 - \sqrt{\zeta})\epsilon} \right) \\
 &\leq \frac{\sqrt{G^2 + \epsilon d}}{\alpha\sqrt{T}} \left(f(\theta_1) - \underline{f} + \frac{C_2}{1 - \sqrt{\zeta}} + \frac{LG^2\alpha^2}{(1 - \sqrt{\zeta})\epsilon} \right)
 \end{aligned}$$

□